

Portfolio Optimization via Quantum Zeno Dynamics on a Quantum Processor

Dylan Herman,* Ruslan Shaydulin,* Yue Sun,* Shouvanik Chakrabarti, Shaohan Hu,
 Pierre Minssen, Arthur Rattew, Romina Yalovetzky, and Marco Pistoia
Global Technology Applied Research, JPMorgan Chase, New York, NY 10017 USA

Portfolio optimization is an important problem in mathematical finance, and a promising target for quantum optimization algorithms. The use cases solved daily in financial institutions are subject to many constraints that arise from business objectives and regulatory requirements, which make these problems challenging to solve on quantum computers. We introduce a technique that uses quantum Zeno dynamics to solve optimization problems with multiple arbitrary constraints, including inequalities. We show that the dynamics of the quantum optimization can be efficiently restricted to the in-constraint subspace via repeated projective measurements, requiring only a small number of auxiliary qubits and no post-selection. Our technique has broad applicability, which we demonstrate by incorporating it into the quantum approximate optimization algorithm (QAOA) and variational quantum circuits for optimization. We analytically show that achieving a constant minimum success probability in QAOA requires a number of measurements that is independent of the problem size for a specific choice of mixer operator. We evaluate our method numerically on the problem of portfolio optimization with multiple realistic constraints, and observe better solution quality and higher in-constraint probability than the state-of-the-art technique of enforcing constraints by introducing a penalty into the objective. We demonstrate the proposed method on the Quantinuum H1-2 trapped-ion quantum processor, observing performance improvements from circuits with two-qubit gate depths of up to 148.

I. INTRODUCTION

The daily operation of a large financial institution requires solving many classically-hard optimization problems [1, 2]. Among such problems, one of the most important is portfolio optimization. Modern portfolio theory [3] considers the task of finding a portfolio with a desired trade-off between risk and expected return. This task is typically formulated as an optimization problem, which is hard to solve classically in many settings, such as when the variables are required to only take on a discrete set of values. When designing an algorithm for portfolio optimization, a central consideration is the ability to incorporate a general class of constraints. Such constraints can come from regulatory or business considerations, with examples ranging from portfolio-level constraints (including budget and total number of assets) to asset-level constraints (such as minimum holding size).

A commonly considered class of quantum optimization algorithms uses a parameterized quantum evolution to drive the quantum system towards a state encoding the solution of the optimization problem. This class of algorithms includes the quantum approximate optimization algorithm (QAOA) [4, 5] and variational algorithms for optimization [6, 7].

One of the main challenges in applying these quantum algorithms to commercially-relevant optimization problems is the need to enforce the constraints. Concretely, the goal is to prepare a quantum state such that upon measuring it, a high-quality solution that satisfies the constraints is obtained with high probability. Two commonly considered approaches are to encode the constraint

into the objective using a penalty term and to directly restrict the parameterized quantum evolution to the in-constraint subspace. In the first approach, a penalty term is added to the objective so that optimizing the objective requires satisfying the constraint. While such approaches are flexible enough to satisfy most constraints, the quality of the result is sensitive to the choice of the penalty strength [8]. As tuning the penalty strength is difficult in general, this approach often leads to sub-optimal performance in practice [9]. This observation motivates the second approach, i.e., restricting the quantum evolution to the in-constraint subspace.

A number of techniques have been proposed to ensure that the parameterized quantum evolution respects the constraints of the problem. Hadfield et al. [10, 11] proposed the quantum alternating operator ansatz algorithm, which applies pairs of alternating operators to an in-constraint initial state. The first alternating operator (*phase operator*) is diagonal in the computational basis and encodes the objective, and the second operator (*mixing operator* or *mixer*) is non-diagonal and restricts the transitions of probability amplitudes to the computational basis states corresponding to the in-constraint solutions. The problem of constructing a Hamiltonian preserving arbitrary constraints is NP-complete even for linear constraints [12], though explicit constructions are available for some combinatorial optimization problems [10, 11, 13, 14]. In general, constraint-preserving mixers are difficult to implement, even when constructions are available [15, 16]. The cost of implementing the algorithm on hardware can be reduced for a restricted class of problems by combining the phase and mixing operators [17]. If a uniform superposition of in-constraint states can be prepared efficiently, a Grover operator can be used as the mixer [18–20]. Finally, for

* These authors have contributed equally.

problems with an indexable set of feasible states (such as those with Hamming-weight constraints), a continuous-time quantum walk in the solution space can be used as a mixer [21–23]. However, none of these techniques are sufficiently flexible to handle the general case of multiple arbitrary constraints directly. The parity optimization framework [24–28] can natively handle polynomial equality constraints for QAOA-like circuits. However, this framework introduces an auxiliary qubit for every unique monomial term that appears, leading to large space overhead for complex objectives and constraints. All of the techniques mentioned above consider QAOA-like alternating operator circuits, and are not easy to generalize to other variational algorithms.

In this work, we introduce an approach for enforcing multiple arbitrary constraints in quantum optimization. We restrict the quantum evolution to the in-constraint subspace by repeated projective measurements. In each measurement, the value of the constraint is computed onto an auxiliary register, which is then measured. Our technique uses quantum Zeno dynamics, wherein the evolution of the system is restricted to the subspace defined by the repeated projective measurements and transitions outside of this subspace are suppressed. Our approach is applicable to any problem in NPO (the NP optimization complexity class), as the only restriction we impose on the constraints is the existence of an efficient oracle for testing it. We provide explicit constructions for arbitrary combinatorial constraints.

We demonstrate the effectiveness of the proposed technique by applying it to enforcing the constraints in QAOA and the layer variational quantum eigensolver (L-VQE) [29], which is a variational quantum algorithm for optimization. We show analytically that our technique is guaranteed to obtain the optimal in-constraint solution when applied to the digital simulation of the quantum adiabatic algorithm, or equivalently to QAOA in the constrained subspace with sufficiently large depth. We derive an analytical form of the scaling of the number of measurements required to maintain a constant minimum success probability for any parameterized quantum evolution. Furthermore, we provide numerical evidence that our technique, applied to QAOA, provides significant performance improvements over the state-of-the-art method of enforcing the constraint by introducing a penalty term. Finally, we implement QAOA with Zeno dynamics on the Quantinuum H1-2 trapped-ion quantum processor and observe performance improvements from increasing the number of measurements, up to a two-qubit circuit depth of 148. We make all the data presented in this paper available online at <https://doi.org/10.5281/zenodo.7125969>.

The rest of the paper is organized as follows. We introduce relevant background on quantum optimization in Section II A and on quantum Zeno dynamics in Section II B. We define our approach and provide the scaling of the resource requirements in Section III. We present the numerical experiments with QAOA and L-VQE in

Section IV and the experiments on a trapped-ion quantum processor with QAOA in Section V. We conclude with a brief discussion of the results in Section VI.

II. PRELIMINARIES

We begin by briefly introducing the relevant concepts and setting the notation. We undertake the task of minimizing an objective function f defined on the Boolean cube over the set of feasible solutions $\mathcal{F} \subseteq \mathbb{B}^n$:

$$\min_{\mathbf{x} \in \mathcal{F}} f(\mathbf{x}). \quad (1)$$

We consider sets \mathcal{F} of the form $\mathcal{F} = \{\mathbf{x} \in \mathbb{B}^n \mid \bar{g}_j(\mathbf{x}) = 0 \forall j\}$, where $\bar{g}_j(\mathbf{x})$ is an oracle that returns 0 if \mathbf{x} satisfies the j -th constraint and a value strictly greater-than 0 otherwise. This general definition includes most commonly considered problems such as those with equality and inequality constraints.

This constrained optimization problem can be solved by relaxing the constraints and introducing penalty terms as follows:

$$\min_{\mathbf{x} \in \mathbb{B}^n} f_{\text{penalty}} = \min_{\mathbf{x} \in \mathbb{B}^n} f(\mathbf{x}) + \sum_j \lambda_j \bar{g}_j(\mathbf{x}), \quad (2)$$

where $\lambda_j \in \mathbb{R}^+$ are the penalty factors.

Specifically, for an equality constraint $g(\mathbf{x}) = 0$, the penalty function may be written as

$$\bar{g}(\mathbf{x}) = [g(\mathbf{x})]^2.$$

On the other hand, an inequality constraint $g(\mathbf{x}) \geq 0$ can be converted into an equivalent equality constraint $g(\mathbf{x}) - \hat{s} = 0$ by introducing a *slack variable* $\hat{s} \in [0, g_{\max}]$, where $g_{\max} = \max_{\mathbf{x} \in \mathcal{F}} g(\mathbf{x})$. If we assume $g(\mathbf{x})$ can be discretized with a spacing of Δ_g , then \hat{s} can be implemented using $n_{\text{slack}} = \lceil \log_2(g_{\max}/\Delta_g) \rceil$ binary variables $\mathbf{s} = (s_1, \dots, s_{n_{\text{slack}}})^T$, and the resultant equality constraint is $g(\mathbf{x}) - \Delta_g \sum_j 2^{j-1} s_j = 0$. Therefore the penalty function for an inequality constraint can be written as

$$\bar{g}(\mathbf{x}; \mathbf{s}) = \left[g(\mathbf{x}) - \Delta_g \sum_{j=1}^{n_{\text{slack}}} 2^{j-1} s_j \right]^2.$$

The magnitudes of the penalty factors λ_j control how much the constraint violations are penalized. Intuitively, a higher value of λ_j should lead to a higher in-constraint probability. However, in practice, the relationship between the penalty factor, the in-constraint probability and the solution quality may be non-monotonic. This makes choosing λ_j harder. We discuss the difficulty of tuning the penalty factors in Section IV C.

A. Quantum algorithms for approximate optimization

In this work, we focus on the class of quantum optimization algorithms that use a parameterized quantum

evolution to prepare a state, such that the corresponding measurement outcomes contain a high-quality, valid solution to the original optimization problem with high probability. This parameterized state is prepared by applying a parameterized evolution $U(\boldsymbol{\theta})$ to some initial state $|s\rangle$:

$$|\psi(\boldsymbol{\theta})\rangle = U(\boldsymbol{\theta})|s\rangle = \prod_{j=1}^m e^{-i\theta_j H_j} |s\rangle, \quad (3)$$

where H_j is some Hamiltonian, e.g., a tensor product of single-qubit Pauli operators.

Let $C = \sum_{\mathbf{x} \in \mathbb{B}^n} f(\mathbf{x}) |\mathbf{x}\rangle\langle\mathbf{x}|$ be the operator encoding the objective function f on qubits and $C_{\text{penalty}} = \sum_{\mathbf{x} \in \mathbb{B}^n} f_{\text{penalty}}(\mathbf{x}) |\mathbf{x}\rangle\langle\mathbf{x}|$ be the operator encoding the relaxed objective function (2). The figures of merit used to evaluate the quality of a parameter $\boldsymbol{\theta}^*$ obtained by algorithms that employ parameterized circuit (3) are approximation ratios, defined as follows:

$$r = \frac{\langle\psi(\boldsymbol{\theta}^*)| C_{\mathcal{F}} |\psi(\boldsymbol{\theta}^*)\rangle - f^{\max}}{f^{\min} - f^{\max}} \quad (4)$$

and

$$r_{\text{penalty}} = \frac{\langle\psi(\boldsymbol{\theta}^*)| C_{\text{penalty}} |\psi(\boldsymbol{\theta}^*)\rangle - f_{\text{penalty}}^{\max}}{f_{\text{penalty}}^{\min} - f_{\text{penalty}}^{\max}}, \quad (5)$$

where $C_{\mathcal{F}} = \sum_{\mathbf{x} \in \mathcal{F}} f(\mathbf{x}) |\mathbf{x}\rangle\langle\mathbf{x}|$, $f^{\min} = \min_{\mathbf{x} \in \mathcal{F}} f(\mathbf{x})$, $f^{\max} = \max_{\mathbf{x} \in \mathcal{F}} f(\mathbf{x})$, $f_{\text{penalty}}^{\min} = \min_{\mathbf{x} \in \mathbb{B}} f_{\text{penalty}}(\mathbf{x})$, and $f_{\text{penalty}}^{\max} = \max_{\mathbf{x} \in \mathbb{B}} f_{\text{penalty}}(\mathbf{x})$.

This class of algorithms includes QAOA [4, 5, 30] and its generalization, the quantum alternating operator ansatz algorithm [11]. In both algorithms, the parameterized quantum evolution is performed by applying pairs of alternating operators:

$$|\psi(\boldsymbol{\beta}, \boldsymbol{\gamma})\rangle = \prod_j [U_B(\beta_j) U_C(\gamma_j)] |s\rangle, \quad (6)$$

where $U_C(\gamma_j) = e^{-i\gamma_j C}$ is the phase operator, and $U_B(\beta_j)$ is the mixing operator. In the special case of QAOA, the initial state $|s\rangle$ is the uniform superposition over all computational basis states and the mixing operator U_B is set to be $U_B(\beta_j) = e^{-i\beta_j B}$, where $B = \sum_k x_k$ is a sum of single-qubit Pauli-X operators. In quantum alternating operator ansatz, U_B and $|s\rangle$ are allowed to be arbitrary, and are typically set such that the resulting state $|\psi(\boldsymbol{\beta}, \boldsymbol{\gamma})\rangle$ preserves the constraints, in the sense that every measurement outcome \mathbf{x} belongs to \mathcal{F} . In this paper, we consider QAOA with an arbitrary mixing Hamiltonian B , defined in Ref. [11] as ‘‘Hamiltonian-based QAOA.’’ In the remainder of the paper, the acronym QAOA will be used to denote this version of the algorithm.

In addition to QAOA, we consider L-VQE [29], which is a version of VQE with the hardware-efficient layered pa-

rameterized circuit tailored towards optimization problems. L-VQE uses the parameterized circuit of the form

$$\prod_{j=1}^p [U_{\text{NN}}(\boldsymbol{\theta}_j)] V(\boldsymbol{\theta}_0) |0\rangle, \quad (7)$$

where U_{NN} consists of nearest-neighbor CNOT’s and single-qubit RY’s, and V is a layer of single-qubit RY’s. The reader is referred to Ref. [29] for the precise definition of the circuit. While the circuit includes non-parameterized CNOT’s, it is easy to write it equivalently in the form of Equation (3) by pushing RY through the control of the CNOT and noting that $\text{RY}(\theta) = e^{-i\frac{\theta}{2}Y}$ and $\text{CNOT}_{1,2} \text{RY}_2(\theta) \text{CNOT}_{1,2} = e^{-i\frac{\theta}{2}Z_1 Y_2}$. Here, Y_j and Z_j denote a single-qubit Pauli-Y and Pauli-Z, respectively, acting on the j -th qubit.

B. Quantum Zeno dynamics

The quantum Zeno effect (QZE) [31, 32] is named after Zeno’s paradox [33], which regards the continuous observation of a moving arrow. Zeno’s paradox states that an arrow cannot move if no time has elapsed since the point it was last observed. If the time difference between observations is Δt , continuous observation occurs in the limit of $\Delta t \rightarrow 0$. Under continuous observation, no time elapses between observations, and during each observation the arrow is not moving; thus, no overall movement is possible. The analogue in quantum mechanics is a consequence of the Schrödinger equation. We first introduce a simpler one-dimensional version, in which the quantum state is ‘‘frozen’’ by repeated measurements, and then present a more general case in which the dynamics of the system are restricted to a particular ‘‘Zeno subspace.’’

Suppose a time-dependent quantum state is evolved in a finite-dimensional Hilbert space \mathcal{H} from some initial state $|\psi_0\rangle$ under the action of some Hamiltonian H for time t . Define a projective measurement \mathcal{P} given by a pair of complement projections $P = |\psi_0\rangle\langle\psi_0|$ and $Q = I - P$, which acts on a density operator ρ as

$$\mathcal{P}\rho = P\rho P + Q\rho Q.$$

If we carry out N repeated projective measurements \mathcal{P} at a time interval of t/N , then the probability that the system remains in the initial state is

$$\begin{aligned} p(t) &= \|Pe^{-iHt/N}|\psi_0\rangle\|_2^{2N} \\ &= \left[|\langle\psi_0|e^{-iHt/N}|\psi_0\rangle|^2\right]^N \\ &= \left[1 - (t/N\tau_Z)^2\right]^N + O(N^{-2}) \xrightarrow{N \rightarrow \infty} 1, \end{aligned}$$

where $\tau_Z^{-2} = \langle\psi_0|H^2|\psi_0\rangle - \langle\psi_0|H|\psi_0\rangle^2$ is the ‘‘Zeno time’’ quantifying how often the measurements need to be taken. As the frequency at which the measurements are performed increases without bound, the probability of remaining in the initial state approaches one.

Quantum Zeno dynamics (QZD) [34–37] considers the more general case where the evolution of the state is constrained to a subspace of dimension greater than one. Thus the projective measurement \mathcal{P} can contain multiple projections with ranks all greater than one. Specifically,

$$\mathcal{P}\rho = \sum_{j=1}^k P_j \rho P_j, \quad (8)$$

where $\sum_{j=1}^k P_j = \mathbf{I}$, and P_j is a projection onto some subspace $\mathcal{H}_j = P_j \mathcal{H}$ of dimensionality $\text{Tr}(P_j) \geq 1$. Informally, QZD states that if the evolution starts in \mathcal{H}_j and the measurement \mathcal{P} is performed sufficiently often, then the system will remain in \mathcal{H}_j with high probability.

Consider an initial state ρ_0 , after N projective measurements by \mathcal{P} , the state of the system is given by

$$\rho(t) = \mathcal{U}(t)\rho_0\mathcal{U}(t)^\dagger, \quad (9)$$

where $\mathcal{U}(t) = (\mathcal{P}e^{-iHt/N})^N$ and $p(t) = \text{Tr}(P_j\rho(t))$ is the probability of the system remaining in \mathcal{H}_j after evolving for time t . Note that

$$\begin{aligned} \mathcal{U}(t) &= \left(\mathcal{P}e^{-iHt/N}\right)^N \\ &= (\mathcal{P}(\mathbf{I} - iHt/N + O(N^{-2})))^N \\ &= (\mathbf{I} - i\mathcal{P}Ht/N + O(N^{-2}))^N \\ &= (\mathbf{I} - i\mathcal{P}Ht/N)^N + O(N^{-1}) \quad (10) \\ &\xrightarrow{N \rightarrow \infty} e^{-i\mathcal{P}Ht}\mathcal{P}, \quad (11) \end{aligned}$$

and the dynamics of the system are governed by the “Zeno Hamiltonian” $H_Z = \mathcal{P}H$. Moreover, as $N \rightarrow \infty$, transitions between different subspaces $\{\mathcal{H}_1, \dots, \mathcal{H}_k\}$ of \mathcal{H} are suppressed. This implies if $\rho_0 = P_j\rho_0P_j$ for some $j \in [k] := \{1, \dots, k\}$, then in the limit $N \rightarrow \infty$, it follows that $p(t) \rightarrow 1$, and thus the state will remain in \mathcal{H}_j throughout the evolution. For a more detailed discussion the reader is referred to Refs. [36, 37].

QZE has many applications in algorithms and error mitigation. Childs et al. [38] propose a version of Grover’s search based on QZD that utilizes frequent measurements instead of slow adiabatic evolution. This alternative approach to slow evolution was also observed in [39]. Somma et al. [40, 41] develop a quantum-enhanced version of the simulated annealing algorithm. Their approach makes use of QZD to ensure that the evolution remains in the instantaneous quantum Gibbs state for varying temperature. Boixo et al. [42] show that for Grover’s algorithm and simulated annealing based on QZD, one could use frequent randomized evolutions instead of measurements (“the randomization method”). The randomization method has also been used to implement algorithms for quantum linear systems [43, 44]. Finally, dynamical decoupling, also called “bang-bang” decoupling [45], is a popular error-mitigation technique that uses QZE to suppress decoherence [37, 46–50].

III. QUANTUM ZENO DYNAMICS FOR CONSTRAINED OPTIMIZATION

We now introduce our approach to enforcing constraints in quantum optimization by repeated non-selective projective measurements. Our method is general, though here we focus on algorithms utilizing parameterized states of the form (3). Let $P_{\mathcal{F}}$ denote the projector onto the subspace spanned by computational basis states corresponding to feasible solutions in \mathcal{F} . We discuss the construction of this operator in Section III C. The measurement \mathcal{P} is a super-operator as defined by Equation (8). Without loss of generality, we can assume $P_1 = P_{\mathcal{F}}$, and define $P_{\mathcal{G}} := \mathbf{I} - P_{\mathcal{F}} = \sum_{j=2}^k P_j$.

We give our main result in Theorem 1, which we use to derive the number of measurements required to enforce constraints in parameterized evolutions of the form given by Equation (3).

Theorem 1. *Let \mathcal{P} be the measurement defined in (8). Suppose a system is evolved from some initial state $\rho_0 = P_j\rho_0P_j$ under the action of a Hamiltonian H , whose distinct eigenvalues are $\xi_{\min} = \xi_1 < \xi_2 < \dots < \xi_d = \xi_{\max}$, for time θ . For $\delta \leq 0.19$, if N applications of \mathcal{P} are performed at equally-spaced intervals with*

$$N = \left\lceil \frac{[\theta(\xi_{\max} - \xi_{\min})]^2}{\ln(1 - 2\delta)^{-2}} \right\rceil, \quad (12)$$

then the probability of measuring a state in \mathcal{H}_j at time θ is lower bounded by $1 - \delta$:

$$\text{Tr}[P_j\rho(\theta)] \geq 1 - \delta, \quad (13)$$

where

$$\rho(\theta) = \mathcal{U}(\theta)\rho_0\mathcal{U}(\theta)^\dagger, \quad \mathcal{U}(\theta) = [\mathcal{P}e^{-iH\theta/N}]^N \quad (14)$$

Remark 1. *Note that since $2\|H\|_2 \geq |\xi_{\max} - \xi_{\min}|$, the bound can be reformulated in terms of the spectral norm of the Hamiltonian. This may be useful as the spectral norm may be easier to bound in practice for complicated Hamiltonians.*

Proof. See Section III B. □

Assume that the initial state $|s\rangle$ respects the constraints, that is $P_{\mathcal{F}}|s\rangle = |s\rangle$. We apply a parameterized unitary $U(\theta)$ to the initial state following Equation (3). To enforce the constraints, we can insert measurements into the parameterized evolution as follows:

$$\mathcal{U}_Z(\theta) = \prod_{k=1}^L \left[\mathcal{P} \prod_{j=1}^{m_k} e^{-i(\theta_{r(k,j)}/N_k)H_{r(k,j)}} \right]^{N_k}, \quad (15)$$

where $r(k,j) = \sum_{t=1}^{k-1} m_t + j$ and each sequence of m_k parameterized evolutions, without a measurement,

is called a *block*. The following corollary provides a sufficient N_k for each block to ensure a desired minimum in-constraint probability. The limiting dynamics, i.e. when $N_k \rightarrow \infty$, $\forall k$, will be different depending on how the blocks are chosen.

Corollary 1. *Let \mathcal{P} be the measurement defined in Equation (8). Let the parameterized evolution defined in Equation (15) evolve the system from some initial state $\rho_0 = P_j \rho_0 P_j$. Then, in order to ensure that*

$$\text{Tr}[P_j \mathcal{U}_Z(\boldsymbol{\theta}) \rho_0 \mathcal{U}_Z(\boldsymbol{\theta})^\dagger] \geq 1 - \delta$$

it suffices to choose

$$N_k = \left\lceil \frac{4L[\sum_{j=1}^{m_k} |\theta_{r(k,j)}|]^2 \max_j \|H_{r(k,j)}\|_2^2}{\tau(\delta)} \right\rceil, \quad (16)$$

where

- $\tau(\delta) = \ln(1 - 2\delta)^{-2}$ if $H_{r(k,j)}$ pairwise commute,
- $\tau(\delta) = \ln(1 - \delta)^{-1.78}$ otherwise,

and $\delta \leq 0.19$. In addition, the asymptotic dynamics is

$$\prod_{k=1}^L e^{-i\mathcal{P}\mathbf{H}_k \cdot \boldsymbol{\theta}_k} \mathcal{P}, \quad (17)$$

where \mathcal{P} acts element-wise on the vector $\mathbf{H}_k = (H_{(k,1)}, \dots, H_{(k,m_k)})^\top$ and $\boldsymbol{\theta}_k = (\theta_{(k,1)}, \dots, \theta_{(k,m_k)})$.

Proof. For simplicity, consider a single block of size m :

$$\mathcal{U}_Z(\boldsymbol{\theta}) = \left[\prod_{j=1}^m e^{-i(\theta_j/N)H_j} \right]^N. \quad (18)$$

First, suppose that the elements of $\{H_j\}_{j=1}^m$ do not all pairwise commute. Then, according to [51, Proposition 9]:

$$\begin{aligned} & \left\| \prod_{j=1}^m e^{-i(\theta_j/N)H_j} - e^{-i\sum_{j=1}^m (\theta_j/N)H_j} \right\|_2 \\ & \leq \frac{1}{2N^2} \sum_{j=1}^m \left\| \left[\sum_{j'=j+1}^m \theta_{j'} H_{j'}, \theta_j H_j \right] \right\|_2 \end{aligned} \quad (19)$$

This implies that

$$\begin{aligned} & \left\| \mathcal{U}_Z(\boldsymbol{\theta}) - \left[\mathcal{P} e^{-i\sum_{j=1}^m (\theta_j/N)H_j} \right]^N \right\|_2 \\ & \leq \frac{1}{2N} \sum_{j=1}^m \left\| \left[\sum_{j'=j+1}^m \theta_{j'} H_{j'}, \theta_j H_j \right] \right\|_2 \\ & \leq \frac{\left[\sum_{j=1}^m |\theta_j| \right]^2 \max_j \|H_j\|_2^2}{N}. \end{aligned} \quad (20)$$

Then

$$\begin{aligned} & \|P_{\mathcal{G}} \mathcal{U}_Z(\boldsymbol{\theta}) |\psi\rangle\|_2^2 \leq \\ & \left(\left\| P_{\mathcal{G}} \left[\mathcal{P} e^{-i\sum_{j=1}^m (\theta_j/N)H_j} \right]^N |\psi\rangle \right\|_2 \right. \\ & \left. + \frac{\left[\sum_{j=1}^m |\theta_j| \right]^2 \max_j \|H_j\|_2^2}{N} \right)^2. \end{aligned} \quad (21)$$

If we choose

$$N = \left\lceil \frac{4 \left[\sum_{j=1}^m |\theta_j| \right]^2 \max_j \|H_j\|_2^2}{\ln(1 - \delta)^{-2\alpha}} \right\rceil, \quad (22)$$

then for $\alpha \leq 1$, Theorem 1 with Remark 1 implies that the out-of-constraint probability is at most

$$\begin{aligned} & \|P_{\mathcal{G}} \mathcal{U}_Z(\boldsymbol{\theta}) |\psi\rangle\|_2^2 \leq \frac{\delta}{2} \\ & + \alpha \frac{\sqrt{\delta}}{2} \ln(1 - \delta)^{-2} + \frac{\alpha^2}{16} \ln^2(1 - \delta)^{-2} \end{aligned} \quad (23)$$

$$\leq \frac{\delta}{2} + \frac{\delta}{2} \left[\alpha + \frac{\alpha^2}{8} \right], \quad (24)$$

where $\delta \leq 0.19$. If $\alpha = 0.89$, then

$$\|P_{\mathcal{G}} \mathcal{U}_Z(\boldsymbol{\theta}) |\psi\rangle\|_2^2 < \delta. \quad (25)$$

To compensate for the decay of the success probability after L blocks, each N_k must be multiplied by L .

Lastly, for the pairwise commuting case, from Equation (10)-(11) we get

$$\begin{aligned} \mathcal{U}_Z(\boldsymbol{\theta}) &= \left[\mathcal{P} \prod_{j=1}^m (I - i(\theta_j/N)H_j + O(N^{-2})) \right]^N \\ &= \left[\mathcal{P} \left(I - i \sum_{j=1}^m (\theta_j/N)H_j + O(N^{-2}) \right) \right]^N \end{aligned} \quad (26)$$

$$\xrightarrow{N \rightarrow \infty} e^{-i\sum_{j=1}^m \mathcal{P} H_j \theta_j} \mathcal{P} = e^{-i\mathcal{P}\mathbf{H} \cdot \boldsymbol{\theta}} \mathcal{P}. \quad (27)$$

Thereby the dynamics are described by the Zeno Hamiltonian $\mathbf{H}_Z = \mathcal{P}\mathbf{H}$, where \mathcal{P} acts element-wise on the vector $\mathbf{H} = (H_1, \dots, H_m)^\top$. The limiting dynamics of L blocks is the product of these limits.

If the elements of $\{H_j\}_{j=1}^m$ pairwise commute, then there is no Trotter error, and $\alpha = 1$ without the need to halve δ . The limiting dynamics follows trivially as well. \square

Remark 2. *For combinatorial optimization problems, constraint-preserving measurements that correspond to different constraints always commute. Thus $\mathcal{P}_{\mathcal{F}}$ can be implemented as a composition of measurements corresponding to different constraints.*

Corollary 2. Let \mathcal{P} be the measurement defined in Equation (8). Let the parameterized evolution defined in Equation (15) evolve the system from some initial state $\rho_0 = P_j \rho_0 P_j$. Then, in order to ensure that

$$\text{Tr}[P_j \mathcal{U}_Z(\theta) \rho_0 \mathcal{U}_Z(\theta)^\dagger] \geq 1 - \epsilon$$

it suffices to fix δ , choose N_k according to Corollary 1 and repeat the Zeno evolution at most $\log(1/\epsilon)$ times.

Proof. Since we can efficiently check whether the parameterized evolution preserved the constraints by measuring \mathcal{P} , $\log(1/\epsilon)/\log(1/\delta) < \log(1/\epsilon)$ repetitions suffice to ensure that the outcome of at least one of the repetitions is in constraint with probability at least $1 - \epsilon$. \square

These results imply that for most practical cases, e.g. when H_j are Pauli operators as in the cases of QAOA and hardware-efficient parameterized circuits, the number of measurements scales at most quadratically in the circuit depth and width. Thus, QZD can be used to efficiently constrain parameterized evolution for quantum optimization.

A. Constrained QAOA via Zeno dynamics

We now discuss the application of QZD to QAOA. In a QAOA circuit, the phase operator $U_C(\gamma)$ is diagonal in the computational basis and cannot violate constraints. Therefore the measurements only need to be added to the mixing operator. The full circuit then becomes

$$\mathcal{U}_{Z\text{-QAOA}}(\beta, \gamma) = \prod_j [\mathcal{U}_B(\beta_j, N_j) U_C(\gamma_j)], \quad (28)$$

where

$$\mathcal{U}_B(\beta_j, N_j) = \left[\mathcal{P} e^{-i \frac{\beta_j}{N_j} B} \right]^{N_j}. \quad (29)$$

As the mixing Hamiltonian B is known, we can derive explicitly the number of measurements required to maintain a constant success probability. We observe that for any mixer this number of measurements grows linearly with the number of QAOA layers, and for commonly considered mixers, the number of measurements grows no more than quadratically with the number of qubits.

Corollary 3. Let $\mathcal{U}_{Z\text{-QAOA}}(\beta, \gamma)$ denote the QAOA circuit on n qubits with N measurements added to each mixing operator as defined in (28). Let the initial state $\rho_0 = |s\rangle\langle s|$ be in-constraint. Then N_j measurements suffice to maintain a probability of obtaining an in-constraining measurement outcome of at least $1 - \delta$, where

- if $B = \sum_{k=1}^n x_k$, then $N_j = \left\lceil \frac{p\beta_j^2 n^2}{\ln [1-2\delta]^{-\frac{1}{2}}} \right\rceil$
- if $B = |+\rangle\langle +|$, then $N_j = \left\lceil \frac{p\beta_j^2}{\ln [1-2\delta]^{-2}} \right\rceil$,

where $\delta \leq 0.19$.

Proof. The proof follows from Theorem 1 by noting that for $B = \sum_{k=1}^n x_k$ the range of eigenvalues is integers from $-n$ to n and for $B = |+\rangle\langle +|$ the only eigenvalues are one and zero. For QAOA with p layers, the number of measurements increases by a factor of p . \square

Note that the scaling rule of Corollary 3 implies that the number of measurements will change with β_j and thus each mixer layer.

1. QAOA with Zeno dynamics in the adiabatic limit

If the initial state $|s\rangle$ is the ground state of the mixer Hamiltonian B , QAOA is known to be able to prepare the ground state of the cost Hamiltonian C and thereby solve the problem exactly in the limit of an infinite number of QAOA layers by approximating adiabatic evolution [5]. We now show that this limiting behavior is preserved for constrained QAOA with Zeno dynamics.

Now consider QAOA with constraints enforced by measurement \mathcal{P} as defined in Equation (8), in the Zeno limit, the Zeno mixer Hamiltonian is a sum of the original mixer B projected to the subspaces defined by the projectors constituting \mathcal{P} , i.e.,

$$H_Z = \mathcal{P}B = \sum_{j=1}^k P_j B P_j$$

Concretely, consider the task of using QAOA to approximate the adiabatic evolution under the following time-dependent Hamiltonian:

$$H_s(t) = (1 - s(t))B + s(t)C, \quad (30)$$

where $s : [0, T] \rightarrow [0, 1]$ is the interpolating schedule function. A common schedule function is the linear schedule defined by

$$s(t) = \frac{t}{T}, \quad (31)$$

where T is the evolution time scale. Suppose $T \gg O((\min_s \Delta_n(s))^{-2})$, where $\Delta_n(s)$ is the instantaneous minimum difference between the n -th eigenvalue and any other eigenvalue of $H(s)$. If $\forall s$, it holds that $\Delta_n(s) \neq 0$, then the quantum adiabatic theorem [52] implies:

$$\mathcal{T} \exp \left(\int_0^T H_s(t) dt \right) |\phi_n(0)\rangle = |\phi_n(T)\rangle. \quad (32)$$

In the Zeno case, we consider

$$H_s(t) = (1 - s(t))H_Z + s(t)\mathcal{P}C. \quad (33)$$

Consider the QAOA operator with only one measurement per layer, i.e., $N_j = 1, \forall j$ in (28):

$$\mathcal{U}(p) = \prod_{j=1}^p \mathcal{P} \mathcal{U}_B(\beta_j) \mathcal{U}_C(\gamma_j). \quad (34)$$

Now it is easy to recover the parameters β_j, γ_j giving the limit. From the definition of the product integral [53] it follows that

$$\begin{aligned} & \mathcal{T} \exp \left(i \int_0^T H_s(t) dt \right) \\ &= \lim_{p \rightarrow \infty} \prod_{j=1}^p \exp \left(i \frac{T}{p} H_s \left(\frac{jT}{p} \right) \right) \\ &= \lim_{p \rightarrow \infty} \prod_{j=1}^p \exp \left(i \frac{T}{p} \left[\left(1 - \frac{j}{p} \right) \mathcal{P}B + \left(\frac{j}{p} \right) \mathcal{P}C \right] \right) \\ &= \lim_{p \rightarrow \infty} \prod_{j=1}^p \mathcal{P} \exp \left(i \frac{T}{p} \left(1 - \frac{j}{p} \right) B \right) \exp \left(i \frac{jT}{p^2} C \right), \quad (35) \end{aligned}$$

where the third equality follows from expanding to the first order in $\frac{T}{p}$ and that $\frac{j}{p}$ and $1 - \frac{j}{p}$ are bounded by 1.

Thus if $\rho_n(0) = |\psi_n(0)\rangle\langle\psi_n(0)|$ is an n -th eigenstate of H_Z then

$$\rho_n(T) = \lim_{p \rightarrow \infty} \mathcal{U}(p) \rho_n(0), \quad (36)$$

where $\rho_n(T)$ is pure and is an n -th eigenstate of $\mathcal{P}C$. Thus with $\beta_j = -\frac{T}{p} \left(1 - \frac{j}{p} \right)$ and $\gamma_j = -\frac{jT}{p^2}$ as $p \rightarrow \infty$, QAOA with Zeno dynamics approaches the adiabatic limit and recovers the optimal solution.

2. Mitigating mixer limitations in the Zeno limit

While evolution under $P_{\mathcal{F}}BP_{\mathcal{F}}$ is guaranteed to preserve the in-constraint subspace, it may inhibit transitions between states in \mathcal{F} that were allowed with B . This is because states in \mathcal{F} may be connected by B through a path that passes through states not in \mathcal{F} . To see this, consider a simple example of the two-qubit mixer $B_2 = x_1 + x_2$ and the in-constraint space $\mathcal{F} = \{|01\rangle, |10\rangle\}$. In the Zeno limit, the mixing operator evolution in the in-constraint subspace is generated by $P_{\mathcal{F}}B_2P_{\mathcal{F}}$, which equals the zero matrix. Thus, the mixing unitary becomes the identity operator and the dynamics become trivial. In general, if there is no path between two computational basis states $|j\rangle, |k\rangle \in \mathcal{F}$ in the graph defined by B , the continuous-time quantum walk defined by the mixing operator cannot move probability amplitude from $|k\rangle$ to $|j\rangle$. Whether the transitions between in-constraint states are suppressed in the Zeno limit is in general dependent on the in-constraint space \mathcal{F} .

One way to avoid the issue of suppressed transitions is by choosing a mixer B with a complete connectivity graph among computational basis states, i.e., $B = |+\rangle\langle+|$. This mixer is also known as the complete-graph mixer [18, 54]. It has been conjectured [54] that mixers with high connectivity, such as the $B = |+\rangle\langle+|$, can at best produce a Grover-like speedup since they do not make use of the structure of the cost operator. While it

is unclear if this conjecture is true, we emphasize that our approach can utilize any mixer and can efficiently enforce constraints as long as the difference between the maximum and minimum eigenvalues of the mixer is polynomial in the number of qubits.

B. Proof of Theorem 1

In this Section we derive our main result, Theorem 1, for the number of measurements required to maintain a constant success probability. We additionally give an explicit example of a projector and initial state (43) that saturate the lower bound on the success probability in Lemma 1.

Lemma 1. *Let H be a Hermitian matrix. Then*

$$\begin{aligned} \min_{P, |\psi\rangle \in \text{Im}(P)} \|Pe^{-i\theta H}|\psi\rangle\|_2^2 &= \cos^2 \left(\frac{\xi_{\max} - \xi_{\min}}{2} \theta \right) \\ \forall \theta \in \mathbb{R}, |\theta| &\leq \frac{\pi}{\xi_{\max} - \xi_{\min}}, \end{aligned}$$

where P is an orthogonal projector and ξ_{\max} and ξ_{\min} are the largest and smallest eigenvalues of H .

Proof. Suppose H has the following eigendecomposition

$$H = \sum_{k=1}^d \xi_k Q_k,$$

where ξ_k are the unique eigenvalues of H (including 0 if H is not full rank) and $\{Q_k\}_{k=1}^d$ is the complete set of projectors onto the corresponding eigenspaces. Therefore

$$\begin{aligned} p(\theta) &= \|Pe^{-i\theta H}|\psi\rangle\|_2^2 \\ &\geq \|\langle\psi|e^{-i\theta H}|\psi\rangle\|_2^2 \\ &= |\langle\psi|e^{-i\theta H}|\psi\rangle|^2 \\ &= \sum_{j,k=1}^d e^{i\theta(\xi_j - \xi_k)} \langle\psi|Q_j|\psi\rangle \langle\psi|Q_k|\psi\rangle \\ &= \sum_{j,k=1}^d \cos(\theta(\xi_j - \xi_k)) \langle\psi|Q_j|\psi\rangle \langle\psi|Q_k|\psi\rangle \\ &= \sum_{j,k=1}^d c_{jk} x_j x_k, \quad (37) \end{aligned}$$

where $c_{jk} = \cos(\theta(\xi_j - \xi_k))$, $x_j = \langle\psi|Q_j|\psi\rangle \geq 0$. Note that the second to the last equality follows from

$$\begin{aligned} & e^{i\theta(\xi_j - \xi_k)} x_j x_k + e^{i\theta(\xi_k - \xi_j)} x_k x_j \\ &= \cos(\theta(\xi_j - \xi_k)) x_j x_k + \cos(\theta(\xi_k - \xi_j)) x_k x_j. \end{aligned}$$

Let C be the matrix with elements c_{jk} at the j -th row and k -th column. Then using simple trigonometric identities, it can be shown that

$$C = \mathbf{v}(\theta)\mathbf{v}(\theta)^T + \mathbf{v} \left(\frac{\pi}{2} - \theta \right) \mathbf{v} \left(\frac{\pi}{2} - \theta \right)^T \quad (38)$$

where

$$\mathbf{v}(\theta) = (\cos(\xi_1\theta), \dots, \cos(\xi_d\theta))^T. \quad (39)$$

Since C is the sum of positive semi-definite matrices, it too is positive semi-definite.

Therefore, minimizing $p(\theta)$ is equivalent to solving the following convex constrained minimization problem

$$\min_{\mathbf{x} \in \mathcal{S}} \mathbf{x}^T C \mathbf{x}, \text{ where } \mathcal{S} := \{\mathbf{x} \in \mathbb{R}_+^d \mid \|\mathbf{x}\|_1 = 1\}, \quad (40)$$

$\mathbf{x} = (x_1, \dots, x_d)^T$ and thus a sufficient condition [55, Theorem 2.2.5] for \mathbf{x}^* to be the optimum is

$$\mathbf{x}^{*\top} C (\mathbf{x} - \mathbf{x}^*) \geq 0, \quad \forall \mathbf{x} \in \mathcal{S} \quad (41)$$

Consider the following trial solution

$$\begin{aligned} x_{\min}^* &= x_{\max}^* = \frac{1}{2}, \\ x_j^* &= 0 \quad \forall j \notin \{\min, \max\}. \end{aligned} \quad (42)$$

We have that $\forall \mathbf{x} \in \mathcal{S}$

$$\begin{aligned} &2\mathbf{x}^{*\top} C (\mathbf{x} - \mathbf{x}^*) \\ &= (1 + c_{\max, \min})(x_{\max} + x_{\min} - 1) \\ &\quad + \sum_{j \notin \{\min, \max\}} x_j (c_{\max, j} + c_{\min, j}) \\ &= (1 - x_{\max} - x_{\min}) \left[\sum_{j \notin \{\min, \max\}} (c_{\max, j} + c_{\min, j}) \right. \\ &\quad \left. - (1 + c_{\max, \min}) \right] \end{aligned}$$

Also for $|\theta| \leq \frac{\pi}{\xi_{\max} - \xi_{\min}}$, we have $c_{j,k} \geq c_{\max, \min}$, and thus

$$\begin{aligned} 1 + c_{\min, \max} &= 2 \cos^2 \left(\frac{\xi_{\max} - \xi_{\min}}{2} \theta \right) \\ &\leq 2 \cos \left(\frac{\xi_{\max} - \xi_{\min}}{2} \theta \right) \cos \left(\frac{\xi_{\max} + \xi_{\min} - 2\xi_j}{2} \theta \right) \\ &= c_{\max, j} + c_{\min, j}. \end{aligned}$$

Combining the above results, we obtain that $2\mathbf{x}^{*\top} C (\mathbf{x} - \mathbf{x}^*) \geq 0$. Thus our choice is optimal.

After, plugging in the optimal choice and noting that all steps are equalities in (37) when $P = |\psi\rangle\langle\psi|$, we obtain:

$$\begin{aligned} &\min_{P, |\psi\rangle \in \text{Im}(P)} \|P e^{-i\theta H} |\psi\rangle\|_2^2 \\ &= \mathbf{x}^{*\top} C \mathbf{x}^* \\ &= \cos^2 \left(\frac{\xi_{\max} - \xi_{\min}}{2} \theta \right). \end{aligned}$$

Additionally, the result implies that minimization occurs when

$$|\psi\rangle = |\pm_H\rangle := \frac{1}{\sqrt{2}} |\xi_{\max}\rangle \pm \frac{1}{\sqrt{2}} |\xi_{\min}\rangle \quad (43)$$

for any $|\xi_{\max}\rangle \in \text{Im}(Q_{\max})$ and $|\xi_{\min}\rangle \in \text{Im}(Q_{\min})$. \square

Lemma 2. *Let H be a Hermitian matrix. Then*

$$\begin{aligned} &\min_{P, |\psi\rangle \in \text{Im}(P)} \left\| P \left(\mathcal{P} e^{-i\frac{\theta}{N} H} \right)^N |\psi\rangle \right\|_2^2 \\ &= \frac{1}{2} + \frac{1}{2} \left[2 p^* \left(\frac{\theta}{N} \right) - 1 \right]^N \\ &\quad \forall \theta \in \mathbb{R}, \quad |\theta| \leq \frac{\pi N}{\xi_{\max} - \xi_{\min}}, \end{aligned}$$

where \mathcal{P} is a projective measurement as defined in Equation (8) with projectors P and $I - P$,

$$p^* \left(\frac{\theta}{N} \right) = \cos^2 \left(\frac{\xi_{\max} - \xi_{\min}}{2N} \theta \right),$$

and ξ_{\max} and ξ_{\min} are the largest and smallest eigenvalues of H .

Proof. Consider a fixed θ and some N that satisfies the hypothesis. The stochastic process formed by random variables indicating whether the system is in $\text{Im}(P)$ or its complement after each evolution segment $\mathcal{P} e^{-i\frac{\theta}{N} H}$ form a two-state Markov chain. According to Lemma 1, the probability of remaining in a “state” on the chain at any point in time is at least

$$p^* \left(\frac{\theta}{N} \right) := \cos^2 \left(\frac{\xi_{\max} - \xi_{\min}}{2N} \theta \right), \quad (44)$$

and this minimum probability is attained at each segment when $|\psi\rangle$ is (43) and $P = |\psi\rangle\langle\psi|$. Because, in this case, the evolution lies in the two-dimensional space spanned by $|\pm_H\rangle$, the result is a Markov chain with transition matrix

$$A(k) = \bar{A} = \begin{pmatrix} p^* & 1 - p^* \\ 1 - p^* & p^* \end{pmatrix}, \quad \forall k \in [N], \quad (45)$$

and $\forall k > N, A(k) = I$.

Therefore the probability of the state remaining in $\text{Im}(P)$ after N steps of the chain is $\bar{A}_{0,0}^N$, or the first diagonal element of the matrix \bar{A} after raising it to the N -th power. Applying diagonalization on \bar{A} , we obtain

$$\bar{A}_{0,0}^N = \frac{1 + (2p^* - 1)^N}{2}. \quad (46)$$

\square

Proof of Theorem 1. For all $\theta \in \mathbb{R}$, such that

$$|\theta| < \frac{N}{\xi_{\max} - \xi_{\min}}, \quad (47)$$

it follows that

$$\begin{aligned} \cos^2 \left(\frac{\xi_{\max} - \xi_{\min}}{2N} \theta \right) &\geq \left(1 - \frac{1}{2} \left[\frac{\theta(\xi_{\max} - \xi_{\min})}{2N} \right]^2 \right)^2 \\ &\geq 1 - \frac{[\theta(\xi_{\max} - \xi_{\min})]^2}{4N^2}. \end{aligned}$$

If we combine this result with Lemma 2, then we obtain

$$\begin{aligned} &\frac{1}{2} + \frac{1}{2} \left[2p^* \left(\frac{\theta}{N} \right) - 1 \right]^N \\ &\geq \frac{1}{2} + \frac{1}{2} \left(1 - \frac{[\theta(\xi_{\max} - \xi_{\min})]^2}{2N^2} \right)^N \\ &\geq \frac{1}{2} + \frac{1}{2} \exp \left(- \frac{[\theta(\xi_{\max} - \xi_{\min})]^2}{2N} \right) \end{aligned} \quad (48)$$

To lower bound this by $1 - \delta$, we can choose N as stated in Theorem 1. Note that to ensure Equation (47) we must have

$$\frac{[\theta(\xi_{\max} - \xi_{\min})]^2}{N} < N, \quad (49)$$

and thus

$$\begin{aligned} &\frac{1}{2} + \frac{1}{2} \exp \left(- \frac{[\theta(\xi_{\max} - \xi_{\min})]^2}{2N} \right) \\ &> \frac{1}{2} + \frac{1}{2} \exp \left(- \frac{N}{2} \right). \end{aligned} \quad (50)$$

At the minimum of value of N , we have

$$\frac{1}{2} + \frac{1}{2} \exp \left(- \frac{1}{2} \right) \lesssim 0.81. \quad (51)$$

□

Figure 1 visualizes how the number of measurements required to maintain a given minimum in-constraint probability, according to Corollary 3, grows with the evolution time β for the $B = \sum_j x_j$ (\times marker) and $B = |+\rangle\langle +|$ (\oplus marker) mixers with 3 qubits. Note that the number of measurements for the mixer $B = \sum_j x_j$ grows with number of qubits and is therefore larger than for $B = |+\rangle\langle +|$. Note that when following the scaling rules of Corollary 3, the number of measurements is multiplied by the number of QAOA layers p .

In Section IV, we observe that for realistic constraints, the number of measurements is significantly lower. This is because the worst-case P_F and $|s\rangle$, i.e., from (43), are far from those encountered in practice. Specifically, the worst-case P_F is rank one (i.e., only one state is in-constraint). A larger in-constraint subspace leads to a lower sufficient number of measurements. Moreover, in

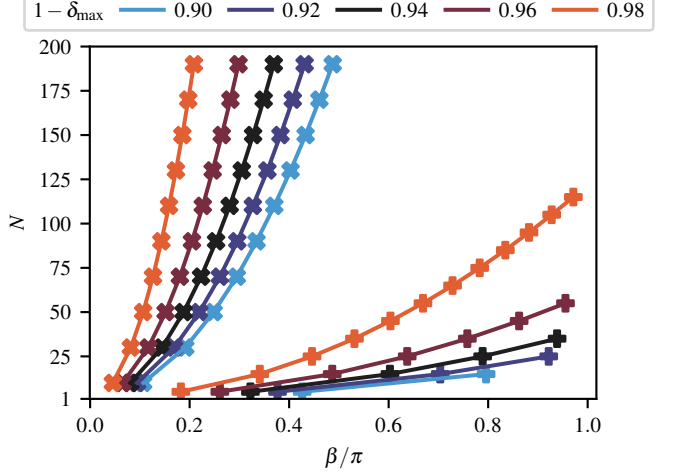


Figure 1. Scaling of number of measurements required to maintain in-constraint probability of at least δ_{\min} for the $B = \sum_j x_j$ (\times marker) and $B = |+\rangle\langle +|$ (\oplus marker) mixers with 3 qubits. Note that this is the scaling required to ensure the desired minimum in-constraint probability for the worst-case initial state and is potentially more pessimistic than what is observed in practice. Many more measurements are required for $B = \sum_j x_j$ as the number of measurements grows quadratically with number of qubits. Note that due to periodicity, $|\beta| \leq \frac{\pi}{2}$ for $B = \sum_j x_j$ and $|\beta| \leq \pi$ for $B = |+\rangle\langle +|$.

practice the initial state is unlikely to align perfectly with the eigenvectors of the mixer. Thus one could consider a relaxed version of the rules provided in Corollary 3 as follows:

$$N = \left\lceil \frac{[\beta(\xi_{\max} - \xi_{\min})]^2}{\eta} \right\rceil, \quad (52)$$

where η is some hyperparameter to be fine tuned. One could always efficiently estimate the in-constraint probability of a QAOA circuit with a fixed η by measuring a single auxiliary qubit indicating whether the final state output by the circuit is in constraint. In the portfolio optimization experiments, we successfully use an η for the $B = \sum_j x_j$ mixer that is orders of magnitude larger than predicted by Corollary 3, requiring a correspondingly smaller number of measurements.

C. Realizing oracles for combinatorial constraints

In this Section, we review the constructions of quantum oracles for implementing polynomial inequality and equality constraints. We use the constructions provided in this Section in the experiments on a trapped-ion quantum computer described in Section V. Since any function on the Boolean cube can be expressed as a polynomial it suffices to only demonstrate constructions for polynomial constraints [56]. In addition, since we are considering problems in NPO we can assume the existence of a

polynomially-sized classical circuit for evaluating any constraints to sufficient precision. Given that all classical basis gates can be represented as polynomials, we can represent our constraint as the composition of polynomially many polynomial functions. Of course, one could also directly implement the classical circuit in a reversible fashion on a quantum device efficiently. For the remainder of this Section, we consider a polynomial function g :

$$g(\mathbf{b}) = \sum_{k=1}^K d_k \prod_{l \in S_k} b_l, \quad (53)$$

where $S_k \subseteq [n]$ and $d_k \in \mathbb{R}$. In addition for $S_k = \emptyset$, $\prod_{l \in S_k} b_l := 1$.

Without loss of generality we can assume that equality constraints are of the form $g(\mathbf{b}) = 0$ and inequality constraints are of the form $g(\mathbf{b}) \geq 0$. We assume that there exists an oracle that computes the value of $g(\mathbf{b})$ into a quantum register (constructions of such oracles are briefly reviewed in Sections III C 1, III C 2). For an equality constraint, we implement the constraint-enforcing measurement by simply measuring the entire register. A projection onto the in-constraint subspace implies that we have observed a 0 in the register. For an inequality constraint, we measure the qubit corresponding to the sign, a 0 corresponds to a successful projection, and apply the inverse of the oracle post measurement.

While the above procedure works in general, there are further optimizations that can be made by utilizing quantum conditional logic (QCL). We give an example of such an optimization in Section V. Further optimizations are possible for double-sided inequalities of the form $0 \leq g(\mathbf{b}) < a$, where a is a power of 2. To implement the measurement corresponding to this double-sided inequality, we only need to measure higher-order bits. Since the results of these high-order bits are now classical, we can change the part of the inverse-oracle circuit controlled on these bits to classically-conditioned single-qubit gates. Lastly, because all constraint-preserving measurements can be implemented separately and thus auxiliary qubits can be reused, the required number of auxiliary qubits to implement all constraint-preserving measurements is equal to the maximum amount of auxiliary qubits required by any oracle call.

In the subsections that follow, we present efficient constructions of oracles that can be used to implement polynomial functions. Both of these use techniques that have been presented in prior work. Here we include a brief review for completeness and present the resource analysis for our setting.

1. Review of classical reversible arithmetic circuits

The design of reversible versions of classical arithmetic circuits has been extensively explored and highly optimized constructions are available [57–59]. Such construc-

tions allow one to implement unitary operations for performing arithmetic on quantum registers. Consider fixed-point arithmetic of m bits including digits both before and after the decimal point. Suppose polynomial g has K terms. For each coefficient d_k , we require an n -qubit controlled m -bit adder. A controlled m -bit adder can be implemented with $O(m)$ T gates [60]. Since a multi-controlled Toffoli can be implemented with a T of $O(n)$ [61, 62] and thus the overall multi-controlled adder can be implemented with a T count of $O(n+m)$. The T count for implementing g is $O(K(n+m))$.

2. Review of quantum Fourier arithmetic

In the near term and in the absence of error correction, a more resource efficient approach is to switch to the Fourier basis using the quantum Fourier transform (QFT) and perform the arithmetic in the Fourier basis. This approach has worse asymptotic complexity in T counts, but requires fewer qubits and CNOT gates. We use this approach in the hardware experiments discussed in Section V. The discussion in this Section is based on Ref. [19], though the idea of using the QFT for quantum arithmetic is well-known, see e.g. [63–65].

For $s \in [2^m]$, the QFT on \mathbb{Z}_{2^m} is defined as follows:

$$\text{QFT}_{2^m} : |s\rangle \mapsto \sum_{k \in [2^m]} e^{-i2\pi ks/2^m} |k\rangle. \quad (54)$$

It can be shown [66] that the right-hand side of (54) is a product state and can be expressed in the following form:

$$\bigotimes_{k=1}^m \frac{|0\rangle + e^{-i\pi \frac{s}{2^{m-k}}} |1\rangle}{\sqrt{2}} = F_m \left(\frac{s}{2^m} \right) |+\rangle^{\otimes m}, \quad (55)$$

where

$$F_m(\theta) := \bigotimes_{k=1}^m R(\pi 2^k \theta) \quad (56)$$

implements the desired operation. In addition, $R(\alpha)$ denotes the phase gate $|0\rangle\langle 0| + e^{i\alpha} |1\rangle\langle 1|$. The angle θ is restricted to $[-\frac{1}{2}, \frac{1}{2})$ to avoid overflow and allow for representing negative numbers. Thus, when implementing a polynomial g , we require that its range match the range of θ , i.e., $\|g\|_\infty \leq \frac{1}{2}$. This can always be satisfied by scaling g accordingly.

As an example, we can add two integers a and b , with the conditions $a, b, a+b \in \{-2^{m-1}, \dots, 0, \dots, 2^{m-1}-1\}$, as follows:

$$\text{QFT}_{2^m}^\dagger F_m \left(\frac{a}{2^m} \right) F_m \left(\frac{b}{2^m} \right) |+\rangle^{\otimes m} = |a+b\rangle. \quad (57)$$

Note, the value in the quantum register is really the two's complement of $a+b$. We define the following controlled operation:

$$F_m(\mathbf{b}, \theta) := |\mathbf{b}\rangle\langle \mathbf{b}| \otimes F_m(\theta) + (I - |\mathbf{b}\rangle\langle \mathbf{b}|) \otimes I, \quad (58)$$

where $\mathbf{b} \in \mathbb{B}^n$. For $S_k \subseteq [n]$, let $\mathbf{1}_{S_k} \in \mathbb{B}^n$ denote the indicator vector of S_k . The process for (approximately) loading the value of the polynomial (53) into a quantum register is:

$$(I \otimes \text{QFT}_{2^m}^\dagger) \prod_{k=1}^K F_m(\mathbf{1}_{S_k}, d_k) |\mathbf{b}\rangle |+\rangle^{\otimes m} = |\mathbf{b}\rangle |\tilde{g}(\mathbf{b})\rangle, \quad (59)$$

where by the assumption on the range of g , $|\tilde{g}(\mathbf{b}) - g(\mathbf{b})| \leq 2^{-m}$. The result is stored in an auxiliary quantum register of size $O(m)$. The operation $F_m(\mathbf{b}, \theta)$ requires m n -controlled rotation gates. Thus overall it requires Km n -controlled rotation gates. An $O(n)$ -controlled Toffoli can be implemented with $O(n)$ T's [61, 62] and each controlled rotation can be ϵ -approximately implemented with $O(\log(1/\epsilon))$ T's [67, 68]. Thus, assuming a fixed rotation-gate approximation error the total cost is $O(Kmn)$.

The operation QFT_{2^m} requires $O(m^2)$ gates to be implemented exactly [66] and can be implemented approximately, for a fixed approximation error, on a fault-tolerant device with $O(m \log(m))$ T gates [68]. For equality constraints, since we will be measuring the entire register containing the value $\tilde{g}(\mathbf{b})$, we swap the coherent implementation of the inverse QFT for the semiclassical variant [69, 70]. This semiclassical version of the QFT replaces all two-qubit gates with classically-controlled single qubit gates and requires only a single auxiliary qubit that is repeatedly measured and reset to compute the bits of $\tilde{g}(\mathbf{b})$. Thus, this approach benefits from both mid-circuit measurements and QCL. A fault-tolerant version of this circuit can be approximately implemented with $O(m \log(m))$ T gates [71]. Thus in a fault-tolerant setting the overall T count of the QFT-based approach is $O(Kmn + m \log(m))$.

D. Initial state construction

Our proposed approach is flexible with regards to the choice of the initial state, any initial state that is in constraint suffices. Thus, unlike [18], when using the complete-graph mixer our approach does not require repeated applications of a unitary and its inverse for preparing the uniform superposition of in-constraint states. However, the initial state we use in experiments discussed in Sections. IV, V is the uniform superposition over all computational basis states encoding in-constraint solutions. In general, this superposition is hard to prepare. However, there exist constructions for a wide range of practically relevant cases. If the set of feasible solutions is efficiently indexable, [22, Section IIIB] gives an efficient procedure for the initial state preparation. In the specific case of a Hamming-weight equality or inequality constraint, the uniform superposition over feasible states is a superposition of Dicke states with corresponding Hamming weights, which can be constructed efficiently [72]. Since, our technique does not require the

state preparation method be reversible, we can make use of repeat-until-success schemes.

E. Parameter optimization

The Zeno framework we propose works well with standard techniques used to optimize parameterized quantum circuits. Specifically, as long as each N_r is large enough to ensure the desired minimum in-constraint probability $1 - \delta$ (c.f. Corollary 1) for the given parameter range, the direction of steepest descent will still result in a circuit with the same minimum in-constraint probability. Here we make an assumption that θ remains bounded throughout optimization, which is a valid assumption in practice. This means that both gradient-based and gradient-free local optimization methods can be used with Zeno-augmented hybrid quantum-classical algorithms. A commonly used way to optimize parameterized quantum circuits is to use the parameter-shift rule [73, 74] in conjunction with a gradient-based optimizer. We now show that the Zeno framework works efficiently with the parameter-shift rule.

We consider the task of finding a minimum-eigenvalue state of an observable M using a parameterized quantum evolution consisting of generating Hamiltonians that are also unitary, e.g. L-VQE. We utilize the measurement scheme presented in Equation (15) with the condition that $\forall k, m_k = 1$. Following similar arguments as [73, Section 3], we obtain

$$\begin{aligned} & \frac{\partial}{\partial \theta_r} \text{Tr} \left\{ M \mathcal{U}_Z(\theta) \rho \mathcal{U}_Z^\dagger(\theta) \right\} \\ &= \sum_{k=1}^{N_r} \text{Tr} \left\{ M_k \mathcal{P} \frac{H_r}{N_r} e^{-i \frac{\theta_r}{N_r} H_r} \rho_k + \text{h.c.} \right\} \\ &= \frac{1}{N_r} \sum_{k=1}^{N_r} \left[\text{Tr} \left\{ M \mathcal{U}_Z^{+(r,k)} \rho \mathcal{U}_Z^{\dagger,+(r,k)} \right\} \right. \\ & \quad \left. - \text{Tr} \left\{ M \mathcal{U}_Z^{-(r,k)} \rho \mathcal{U}_Z^{\dagger,-(r,k)} \right\} \right], \end{aligned} \quad (60)$$

where M_k and ρ_k contain terms that have not be differentiated, and $\mathcal{U}_Z^{\pm(r,k)}$ is the same as $\mathcal{U}_Z(\theta)$ except that the evolution at the $\sum_{t=1}^{r-1} N_t + k$ step has a phase shift of $\pm \frac{\pi}{4N_r}$. Thus, whereas the normal parameter-shift requires two expectation evaluations per parameter, Zeno would require $2N_r$. This is the same additional overhead as in the case of a circuit with gates that share parameters.

It also easy to see that the gradient is biased towards minimizing $M_{\mathcal{F}} = P_{\mathcal{F}} M P_{\mathcal{F}}$, i.e. the in-constraint Hamiltonian, as follows:

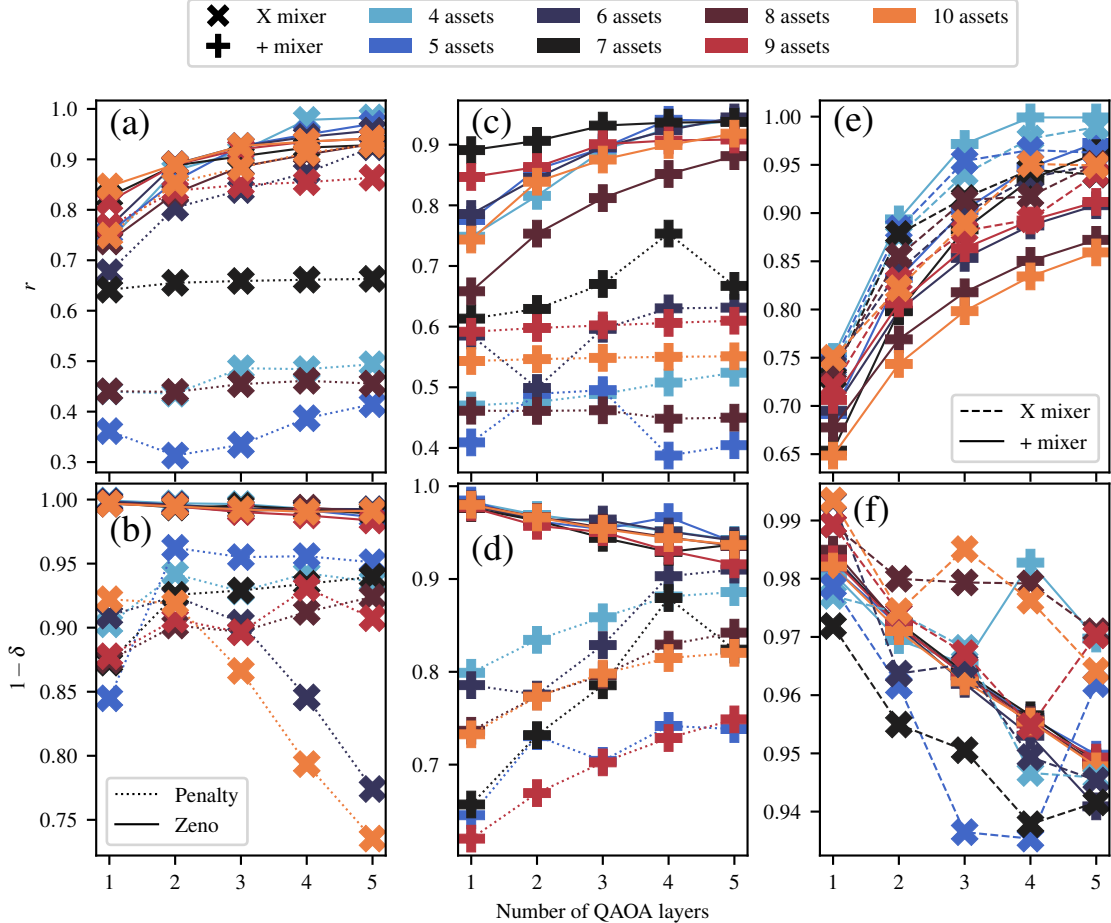


Figure 2. Approximation ratio r and in-constraint probability δ achieved by QAOA with Zeno dynamics (solid lines) and QAOA with constraints enforced using penalty terms (dotted lines) on problems with single (a,b,c,d) and multiple (e,f) constraints. For all single constraint problems QAOA with Zeno dynamics produces superior approximation ratio and in-constraint probability (solid line is above dotted with the same color). As penalty factor tuning is prohibitively difficult for problems with multiple constraints (see Sec. IV C), for these problems only Zeno dynamics results are presented.

$$\begin{aligned}
 & \frac{\partial}{\partial \theta_r} \text{Tr} \left\{ M \mathcal{U}_Z(\theta) \rho \mathcal{U}_Z^\dagger(\theta) \right\} \\
 &= \Pr_{\mathcal{F}} \frac{\partial}{\partial \theta_r} \text{Tr} \left\{ M_{\mathcal{F}} \frac{\mathcal{U}_Z(\theta) \rho \mathcal{U}_Z^\dagger(\theta)}{\Pr_{\mathcal{F}}} \right\} \\
 &+ \Pr_{\mathcal{G}} \frac{\partial}{\partial \theta_r} \text{Tr} \left\{ M_{\mathcal{G}} \frac{\mathcal{U}_Z(\theta) \rho \mathcal{U}_Z^\dagger(\theta)}{\Pr_{\mathcal{G}}} \right\}, \quad (61)
 \end{aligned}$$

where $\Pr_{\mathcal{F}}$ is the probability of projecting onto \mathcal{F} when measuring the parameterized evolution with \mathcal{P} . Lastly, Corollary 1 can be used to ensure $\Pr_{\mathcal{F}} > 1 - \delta$.

IV. NUMERICAL EXPERIMENTS

We now present the numerical experiments showing the power of the proposed method. The technique we

propose is general, though in this section we consider only the problem of portfolio optimization (with both equality and inequality constraints) and only the QAOA and L-VQE algorithms. The parameters in QAOA and VQE were optimized using COBYLA [75] initialized with a large number of random initial points. We compare the results to the state-of-the-art method of encoding constraints by introducing a penalty into the objective, and observe significant improvements in both approximation ratio and in-constraint probability. In addition to better performance, the proposed method does not require complicated tuning of the penalty factor. The data used to generate the figures in this Section is available online at <https://doi.org/10.5281/zenodo.7125969>.

A. Benchmark: portfolio optimization

The particular constrained optimization problems we study numerically arise from the discrete mean-variance Markowitz model [3] and have the following objective function

$$\min_{\mathbf{x} \in \mathcal{F}} q\mathbf{x}^\top \Sigma \mathbf{x} - \boldsymbol{\mu}^\top \mathbf{x}, \quad (62)$$

where \mathcal{F} is defined by some set of constraints on the portfolio. We consider two sets of problems. In the first set, we impose an inequality constraint on the total size of the portfolio ($\sum_j x_j \leq C$). In the second set of problems, in addition to the inequality constraint on portfolio size, we include a constraint on the total expected return ($\sum_j \mu_j x_j \geq R$). For each of the two sets of constraints, we consider seven instances with between four and ten assets, for a total of fourteen instances. In all problem instances $\mathbf{x} \in \mathbb{B}^n$, where n is the number of assets.

B. Zeno dynamics improves quantum optimization performance

Figure 2 presents the comparison between QAOA with Zeno dynamics and QAOA with constraints enforced using penalty factor on fourteen problem instances described in Sec. IV A. We consider QAOA with mixers $B = \sum_j x_j$ (✖ marker) and $B = |+\rangle\langle+|$ (✚ marker), and optimize the QAOA parameters exhaustively. To improve the performance of parameter optimization, we follow Ref. [76] and rescale the cost function so that the gradients with respect to β and γ are roughly of the same magnitude.

For instances with a single constraint, we perform extensive tuning of the penalty factor λ . For multi-constraint problems, the tuning becomes prohibitively expensive. Therefore, we exclude QAOA with constraints enforced through penalties from the comparison for problems with multiple constraints. The choice of the penalty factor and the difficulty of its optimization are discussed in detail in Sec. IV C below.

We observe that Zeno dynamics (solid lines) enables consistently better solution quality and in-constraint probability as compared to QAOA with constraints enforced using a penalty (dotted lines) for all problems considered. Furthermore, Figure 2b shows that for 6 and 10 assets the in-constraint probability drops off rapidly with the number of QAOA layers if the penalty factor is kept constant. This highlights an important limitation of enforcing the constraints via penalties, namely that the penalty factor must be tuned independently for each QAOA depth. In contrast, for QAOA with Zeno dynamics we obtain an explicit rule for how η , from (52), should change with the QAOA depth (see Corollary 3). However, for the numerics shown in Figure 2, we fix η to ensure a constant minimum in-constraint probability per layer. We observe good performance despite η being

a depth-independent constant in this case. We note that since η was held constant while p varied, the in-constraint probability slowly decreases with the number of layers as predicted by Corollary 3. For $B = |+\rangle\langle+|$ mixer, this results in an average number of measurements of ≈ 77 for 6 assets and ≈ 35 for 7 assets. We refer the interested reader to the supplementary raw data for the complete listing of the number of measurements used in each experiment.

We note that the in-constraint probability can be improved arbitrarily for the Zeno dynamics approach by decreasing η , without the need to re-optimize the QAOA parameters. This is due to the objective function landscape becoming independent of η as the Zeno limit is approached. In fact, we observe that transferring parameters from a smaller to a larger number of measurements (larger to smaller η) works well even for practically relevant values of η . Figure 3 shows the approximation ratio r and in-constraint probability with directly optimized QAOA parameters and with pre-optimized parameters transferred from a fixed value of $\eta = 1.6$ (marked with a star in the plot). We observe that for sufficiently small η , transfer works well and the difference in approximation ratio is negligible. Specifically, parameter transfer using the $B = \sum_j x_j$ mixer and a *total* of 33, 75, and 200 measurements results in in-constraint probabilities of at least 85%, 89%, and 96%, respectively for the nine-assets, single-constraint problem at $p = 5$. At the same time, if the number of measurements is very small (η large), the objective function landscape is very different from the landscape in the Zeno limit, and the parameter transfer does not work well. We remark that while the in-constraint probability increases monotonically as η decreases, no such guarantee is given for approximation ratio r . In fact, in Figure 3 we observe that depending on the problem and the circuit depth, r can either increase or decrease with η .

Note that the same approach of boosting the in-constraint probability without re-optimizing the QAOA parameters does not work if the constraints are enforced using penalties. Figure 4 shows that transferring parameters from a fixed value of penalty factor (marked with a star) leads to the approximation ratio rapidly dropping off to random guess. It is however possible that better performance may be achieved by leveraging more sophisticated parameter transfer strategies, such as the rescaling rule proposed for the weighted MaxCut problem [77] or machine learning methods [78].

While for QAOA with Zeno dynamics the approximation ratio r given in Equation (4) increases monotonically with the number of QAOA layers, this is not guaranteed for QAOA with constraints enforced through penalties. This is because the QAOA parameters are chosen with respect to the objective with penalties and the increased expressivity of the higher-depth circuit is only guaranteed to improve the performance with respect to that objective. Figure 5 shows that this is indeed the case and the approximation ratio r_{penalty} given in (5) increases with

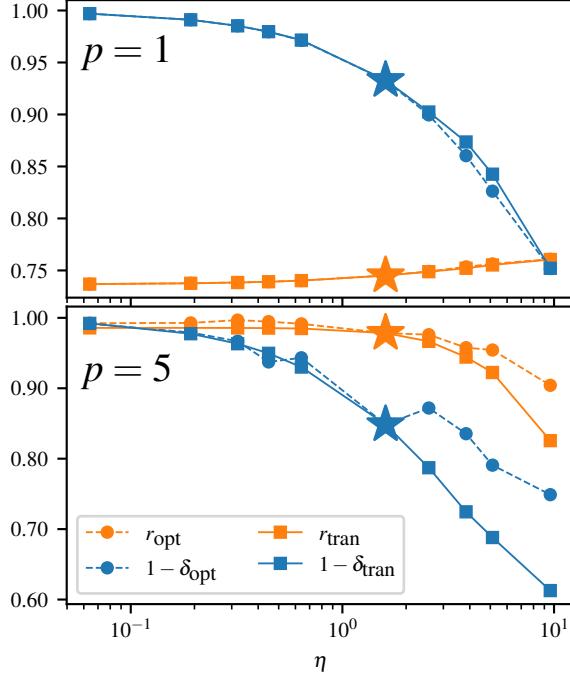


Figure 3. Performance of QAOA with Zeno dynamics and mixer $B = \sum_j x_j$ with directly optimized parameters (r_{opt} , $1 - \delta_{\text{opt}}$) and with parameters transferred from a fixed value of $\eta = 1.6$ (source marked with a star, r_{tran} , $1 - \delta_{\text{tran}}$). For η smaller than 1.6, the difference between performance with optimized and transferred parameters is negligible (dashed line very close to the solid line).

the number of QAOA layers as expected.

Finally, we include the results for Zeno-dynamics L-VQE with $L = 1$ in Equation (15). However, instead of using Corollary 1 to determine a sufficient value for N , we heuristically set the number of measurements to 100. Table I presents the results. As expected, L-VQE achieves high approximation ratio, while Zeno dynamics enables high in-constraint probability. As the total number of measurements is kept fixed for all problems and parameter values, slightly lower in-constraint probability is observed for higher qubit counts. As is the case for QAOA, the in-constraint probability can be increased by increasing the number of measurements.

C. Penalty factor tuning is difficult

An important advantage of our method is the simplicity of hyperparameter tuning, as only η (52) needs to be chosen. This choice is made easy by the theoretical bounds derived in Section III and the monotonic increase of in-constraint probability with decrease in η . This is in sharp contrast with the penalty approach, where the performance crucially depends on the penalty strength, which is hard to tune in general. We now present how the

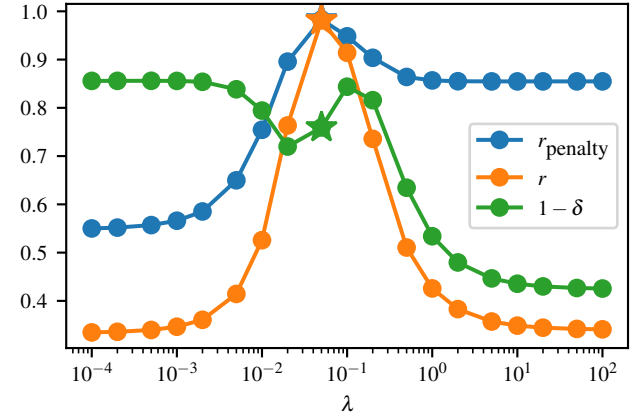


Figure 4. Performance of QAOA with constraints enforced through penalties with parameters transferred from a fixed value of penalty factor $\lambda = 0.1$ (source marked with a star). Approximation ratio drops off to random guess if transferring parameters to values of λ sufficiently different from source.

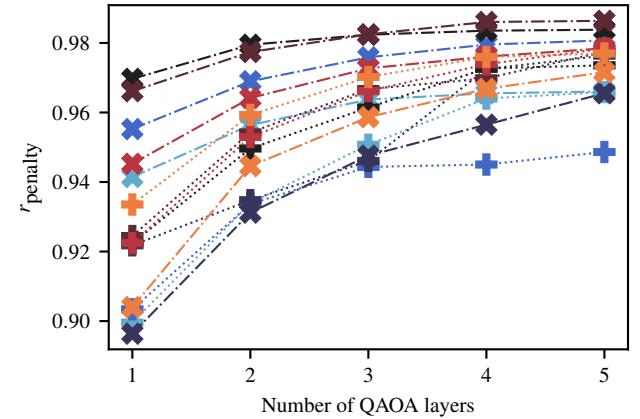


Figure 5. The approximation ratio (5) for the full objective with penalty terms increases monotonically with the number of QAOA layers, as expected. However, the in-constraint approximation ratio (4) is not guaranteed to change monotonically, as seen in Fig. 2a,c. Color denotes the number of assets in the optimization problem, see the legend in Fig. 2.

penalty strength was chosen for the experiments above, and discuss the challenges that arose in doing so.

Figure 6 presents the performance of QAOA on a single-constraint problem enforced using a penalty term with varying penalty factors λ . In the plot, the in-constraint probability $1 - \delta$ monotonically increases with λ , while the approximation ratio r decreases. This indicates a trade-off between r and δ , and hence hyperparameter tuning on λ must be performed in order to obtain a good approximation ratio while meeting requirements on the minimum in-constraint probability. We also observe that for QAOA with small p , δ tends to levels off at a value far below what is achievable by using Zeno dynam-

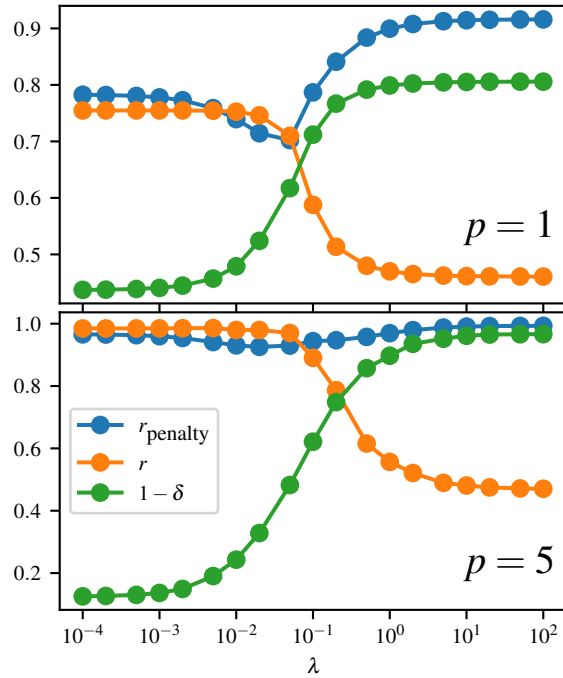


Figure 6. Performance of QAOA with a single constraint enforced through a penalty term with varying penalty factors λ . A trade-off occurs between the approximation ratio r and the in-constraint probability $1 - \delta$.

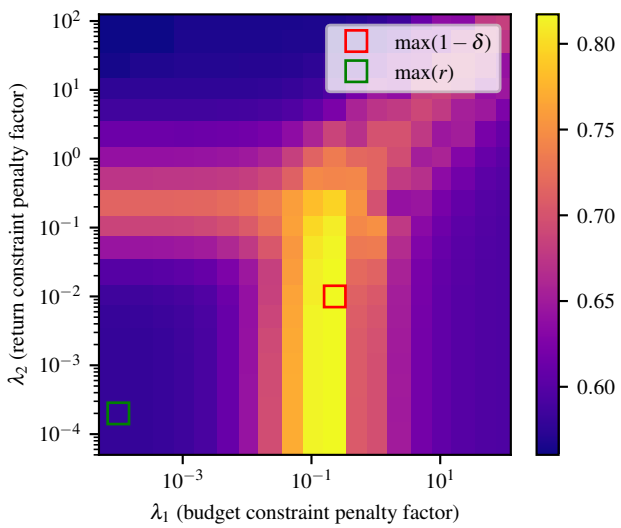


Figure 7. In-constraint probability of optimized solution using the Lagrange penalty approach with varied penalty factors on the maximum budget and minimum return constraints. Figure shows results for $B = |+\rangle\langle +|$ mixer and $p = 3$ QAOA layers, though we observe similar behavior for all mixers and QAOA depths considered.

# assets	Single		Multiple	
	r	$1 - \delta$	r	$1 - \delta$
4	0.995	0.964	0.9996	0.980
5	0.995	0.913	0.977	0.909
6	0.972	0.895	0.964	0.963
7	0.979	0.870	0.917	0.936
8	0.956	0.887	0.948	0.944
9	0.967	0.844	0.961	0.974
10	0.914	0.811	0.910	0.960

Table I. Performance of L-VQE on the benchmark problems. L-VQE obtains high approximation ratio and high in-constraint probability.

ics. For example, the top figure in Figure 6 shows that the highest in-constraint probability achievable with $p = 1$ is around 80% for the problem tested. Given that the approximation ratio with the penalty term r_{penalty} is above 0.9 for the high λ regime, it indicates that the maximum achievable in-constraint probability may be limited by the expressivity of the variational circuit. On the other hand, constraints enforced by Zeno dynamics do not suffer from such problems, as the in-constraint probability can be arbitrarily boosted regardless of the expressivity of the variational circuit (see Figure 3). In the numerical experiments, we choose the value of λ independently for each problem instance with the goal of obtaining a high in-constraint probability δ . Since we show that the factor λ trades off r and δ , both cannot be improved at the same time. This suggests that there does not exist a choice of λ such that QAOA with the penalty method outperforms QAOA with Zeno dynamics.

For problems with multiple constraints, hyperparameter tuning should generally be performed on each penalty factor λ_j included in the relaxed objective (Equation (2)). This means that hyperparameter tuning can quickly become infeasible, as the search space for all λ_j 's grows exponentially with the number of penalty terms. We show in Figure 7 how hyperparameter tuning works with two penalty factors λ_1 and λ_2 corresponding to penalty terms enforcing the budget constraint and the return constraint respectively. The figure shows the in-constraint probability of the optimal solution obtained with varying λ_1 and λ_2 . Similar to the single-constraint case, maximal approximation ratio r and maximal in-constraint probability δ cannot be simultaneously achieved. Specifically, the solutions with the maximal r and maximal $1 - \delta$ have very different values in λ_1 and λ_2 . Moreover, unlike Figure 6, Figure 7 clearly shows the non-monotonic behavior of δ in both λ_1 and λ_2 . In fact, we observe a similar behavior across many of the single- and multi-constraint problems that we have tested, and for both the $B = \sum_j x_j$ and $B = |+\rangle\langle +|$ mixers. This indicates that tuning the penalty factors is indeed difficult in the general case.

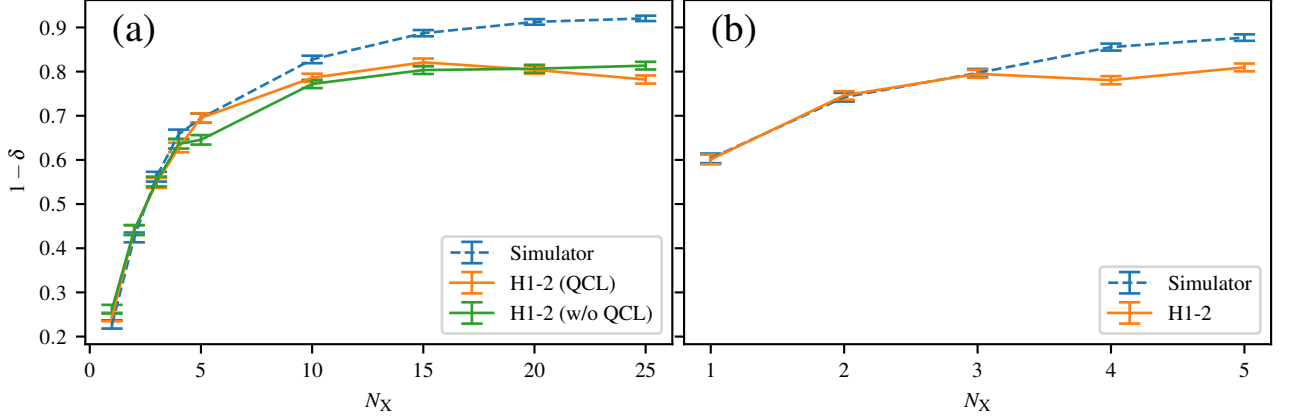


Figure 8. QAOA with $p = 1$ and Zeno dynamics was applied to solve a four-asset problem with an equality constraint $2x_1 - x_2 - x_3 = 0$ (a) and inequality constraint $\sum_{j=1}^4 x_j \leq 2$ (b). The oracles are implemented using arithmetic in the Fourier domain with “QCL” using one auxiliary qubit and “w/o QCL” using three auxiliary qubits. Error bars indicate the standard error of the mean arising from finite sampling (2000 shots). The in-constraint probability $1 - \delta$ grows with the number of measurements.

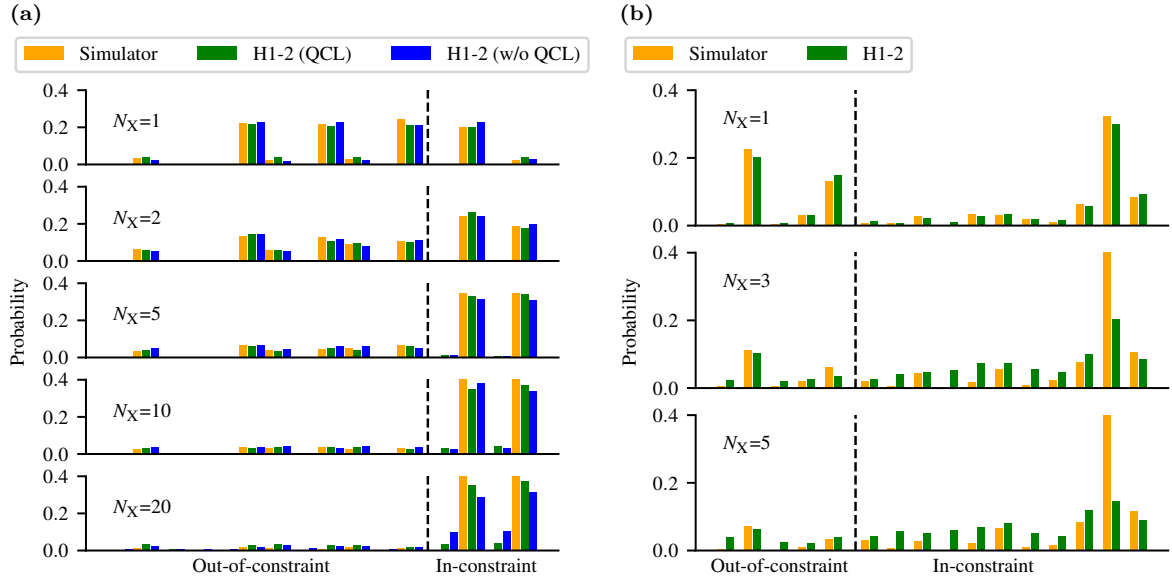


Figure 9. Distribution of measurement results obtained from QAOA applied to the equality- (left) and inequality-constrained (right) problem for different numbers of measurements. Each column corresponds to a computational basis state (either in-constraint or out-of-constraint), and the columns are ordered by objective value (to the right is better). There is strong agreement between the hardware results and results from noise-free simulation.

V. HARDWARE EXPERIMENTS

To demonstrate the near-term feasibility of our approach, we execute QAOA with Zeno dynamics on the Quantinuum H1-2 trapped-ion quantum processor. Our implementation uses the constraint-checking oracles that perform quantum arithmetic in the Fourier domain, following directly the construction in Sec. III C. We observe that increasing the number of measurements im-

proves the in-constraint probability $1 - \delta$, as expected. The improvement from additional measurements continues up to a two-qubit gate depth of 148, at which point the hardware noise prevents further improvements. The circuits executed on hardware are available online at <https://doi.org/10.5281/zenodo.7125969>.

The experiments presented in this Section utilize $p = 1$ QAOA and the $B = \sum_j x_j$ mixer. We use the cost function of the four-assets portfolio optimization problem

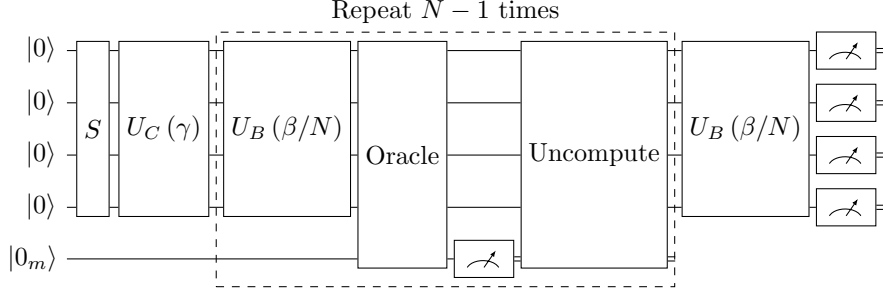


Figure 10. QAOA circuit with Zeno dynamics used in hardware runs for $p = 1$ for four-asset problems. The operator S prepares a uniform superposition over feasible states.

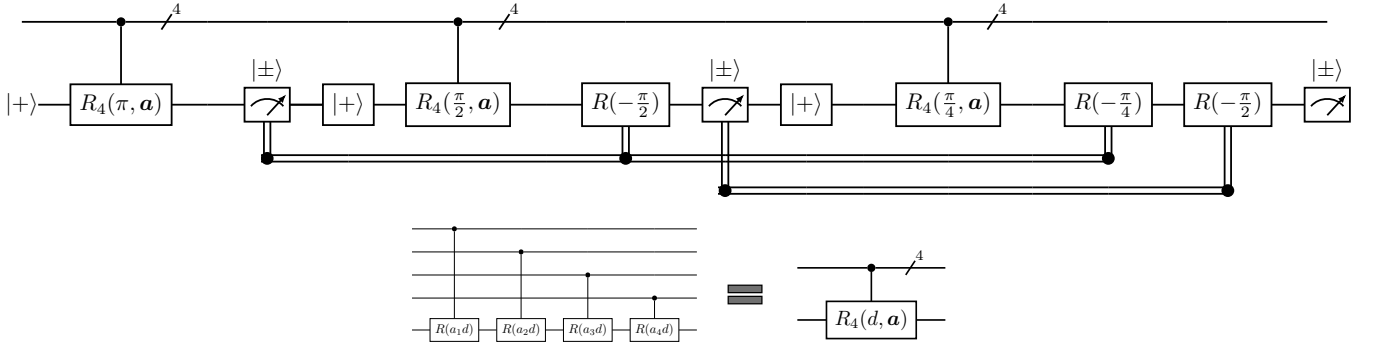


Figure 11. Semiclassical quantum Fourier transform adder for hardware experiments. In addition, $R(\alpha)$ denotes a phase gate. For the equality problem with $a_1 = 2$, $a_2 = -1$, $a_3 = -1$, and $a_4 = 0$. The only uncomputation step for this oracle is to reset the auxiliary qubit to the $|+\rangle$ state.

used in the numerics described in Sec. IV, but apply different constraints. We consider two instances with linear constraints, one with an equality constraint and one with an inequality constraint. Figure 10 shows a high-level circuit diagram. For each problem, the QAOA parameters are first optimized using a noiseless simulator. All circuit executions use 2000 shots and no error mitigation.

The first portfolio optimization instance we consider has an equality constraint on the four binary variables x_1, x_2, x_3, x_4 : $2x_1 - x_2 - x_3 = 0$. As discussed in Section III C 2, the semiclassical QFT can be utilized for equality constraints. The semiclassical QFT makes use of QCL and midcircuit measurements, which are features supported by the H1-2 device. This results in an oracle that uses only one auxiliary qubit, and thus the circuit uses five qubits in total. The circuit for the oracle is shown in Figure 11.

As a comparison, we also implement the coherent QFT on three qubits, resulting in seven qubits in total. After applying the oracle and measuring, all auxiliary qubits are reset to the ground state for the uncompute step. Figure 8a shows the in-constraint probability as a function of the number of projective measurements. Figure 9a shows the distributions of measurement outcomes of QAOA for varying numbers of measurements (N_x), with the outcomes (computational basis states) ordered by the

objective function value. For both implementations, the in-constraint probability improves with the number of measurements up to $N_x \approx 15$. For a higher number of measurements, the hardware noise arising from high circuit depth prevents further improvements in the in-constraints probability $1 - \delta$.

While the QCL and non-QCL implementations both perform similarly, we do note a reduction in the number of two-qubit gates and auxiliary qubits. For QCL and $N_x = 15$, the two-qubit gate depth was 122 and the count was 123. Without QCL, for $N_x = 15$, the two-qubit gate depth was 148 and the count was 165. The similar performance between QCL and non-QCL versions despite the difference in gate count may be due to the higher impact of measurement error on the QCL implementation.

The second portfolio optimization instance we consider has a cardinality (Hamming-weight) inequality constraint $\sum_{j=1}^4 x_j \leq 2$. For this problem, it is necessary to utilize the coherent QFT, and thus QCL does not lead to a resource-requirement reduction. The QFT adder is used to compute $\sum_j x_j - 3$, which requires four qubits to accommodate the range. In addition, unlike the equality-constraint case, the inverse oracle is necessary for uncomputation. The system is in-constraint when the most-significant qubit, i.e., the sign bit, is a one. The circuit for the oracle is shown in Figure 12. Similar to the pre-

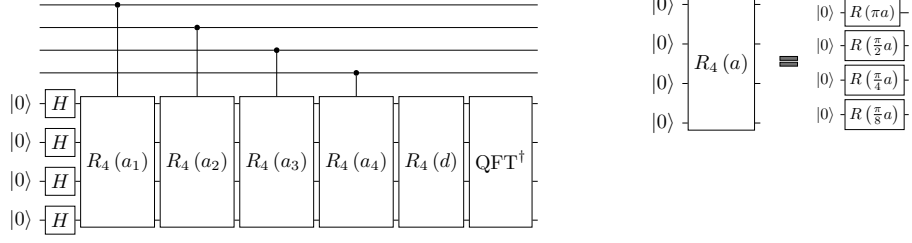


Figure 12. Quantum Fourier transform adder for hardware experiments. In addition, $R(\alpha)$ denotes a phase gate. For the inequality problem, $a_1 = a_2 = a_3 = a_4 = 1$, $d = -3$. The inverse of the oracle is applied after measuring the qubit encoding the sign. Note that here QFT^\dagger does not include swaps as the reordering has been done by rearranging the banks of controlled rotations.

vious run, we plot the in-constraint probability for varying numbers of measurements (Figure 8b), as well as, the measurement distributions obtained from QAOA (Figure 9b). For $N_x = 3$, the two-qubit gate depth is 112 and the count is 186. Similarly to the experiments with the equality constraint, the in-constraint probability δ improves until $N_x = 3$. For a higher number of measurements, the hardware noise prevents further improvements.

Note that the performance deteriorates at a significantly lower N_x for the inequality constraint problem than equality. This occurs even though the two-qubit circuit depth is lower for the inequality case and the two-qubit gate count is not significantly higher. Besides the inclusion of an additional qubit, one potential reason for this is that for the inequality constraint, only one of the auxiliary qubits is measured and then the inverse oracle is applied. This allows for errors to accumulate more and propagate to the rest of circuit. However, in the equality constraint case, after applying the oracles, all auxiliary qubits are measured and then reset to the ground state. In addition, the total gate count happens to be significantly higher for the inequality constraint case.

VI. DISCUSSION

In this work, we propose an approach for enforcing constraints in quantum optimization and demonstrate its

effectiveness by applying it to constrained instances of portfolio optimization in simulation and on a trapped-ion quantum processor. Our technique has two major advantages: the ability to enforce a very general class of constraints and the simplicity of hyperparameter tuning. Two important downsides of our approach are the complexity of implementing the measurement and the possibility of the measurements resulting in trivial dynamics.

Implementing the oracle for a constraint in general requires quantum arithmetic and may lead to high gate count for more complex constraints. At the same time, our hardware experiments show that the overhead is low enough to make our approach viable in the near-term. Reductions in the cost of implementing quantum arithmetic, such as techniques utilizing quantum conditional logic, can further reduce the overhead of the proposed method. Moreover, additional performance improvements can be obtained by leveraging advanced algorithm-specific error mitigation techniques such as the ones recently proposed for QAOA [79, 80].

As discussed in Sec. III A 2, restricting the evolution to the Zeno subspace may result in trivial dynamics for certain mixers. Therefore an important consideration when applying the proposed technique is evaluating whether the particular choice of mixer has this behavior. As this effect would apply generally to all instances with a given class of constraints, the mixer may be analyzed only once for a class of problems.

[1] Dylan Herman, Cody Googin, Xiaoyuan Liu, Alexey Galda, Ilya Safro, Yue Sun, Marco Pistoia, and Yuri Alexeev. A survey of quantum computing for finance. *arXiv preprint arXiv:2201.02773*, 2022.

[2] Romina Yalovetzky, Pierre Minssen, Dylan Herman, and Marco Pistoia. NISQ-HHL: Portfolio optimization for near-term quantum hardware. *arXiv preprint arXiv:2110.15958*, 2021.

[3] Harry M. Markowitz. Portfolio selection. *Journal of Finance*, 7(1):77–91, 1952.

[4] Tad Hogg and Dmitriy Portnov. Quantum optimization. *Information Sciences*, 128(3-4):181–197, 2000.

[5] Edward Farhi, Jeffrey Goldstone, and Sam Gutmann. A quantum approximate optimization algorithm. *arXiv preprint arXiv:1411.4028*, 2014.

[6] Marco Cerezo, Andrew Arrasmith, Ryan Babbush, Simon C Benjamin, Suguru Endo, Keisuke Fujii, Jarrod R McClean, Kosuke Mitarai, Xiao Yuan, Lukasz Cincio, et al. Variational quantum algorithms. *Nature Reviews Physics*, 3(9):625–644, 2021.

[7] Arthur G. Rattew, Shaohan Hu, Marco Pistoia, Richard Chen, and Steve Wood. A domain-agnostic, noise-

resistant, hardware-efficient evolutionary variational quantum eigensolver. *arXiv preprint arXiv:1910.09694*, 2019.

[8] Zhihui Wang, Nicholas C. Rubin, Jason M. Dominy, and Eleanor G. Rieffel. XY-mixers: Analytical and numerical results for the quantum alternating operator ansatz. *Physical Review A*, 101(1), January 2020.

[9] Pradeep Niroula, Ruslan Shaydulin, Romina Yalovetzky, Pierre Minssen, Dylan Herman, Shaohan Hu, and Marco Pistoia. Constrained quantum optimization for extractive summarization on a trapped-ion quantum computer. *arXiv preprint arXiv:2206.06290*, 2022.

[10] Stuart Hadfield. Quantum algorithms for scientific computing and approximate optimization. *Columbia university PhD dissertation*, *arXiv:1805.03265*, 2018.

[11] Stuart Hadfield, Zhihui Wang, Bryan O'Gorman, Eleanor Rieffel, Davide Venturelli, and Rupak Biswas. From the quantum approximate optimization algorithm to a quantum alternating operator ansatz. *Algorithms*, 12(2):34, feb 2019.

[12] Hannes Leipold and Federico M Spedalieri. Constructing driver hamiltonians for optimization problems with linear constraints. *Quantum Science and Technology*, 7(1):015013, November 2021.

[13] Tobias Stollenwerk, Stuart Hadfield, and Zhihui Wang. Toward quantum gate-model heuristics for real-world planning problems. *IEEE Transactions on Quantum Engineering*, 1:1–16, 2020.

[14] Itay Hen and Marcelo S. Sarandy. Driver hamiltonians for constrained optimization in quantum annealing. *Physical Review A*, 93(6), June 2016.

[15] Jeremy Cook, Stephan Eidenbenz, and Andreas Bärtschi. The quantum alternating operator ansatz on maximum k-vertex cover. In *2020 IEEE International Conference on Quantum Computing and Engineering (QCE)*, pages 83–92, 2020.

[16] Franz G Fuchs, Kjetil Olsen Lye, Halvor Møll Nilsen, Alexander J Stasik, and Giorgio Sartor. Constrained mixers for qaoa. *arXiv preprint arXiv:2203.06095*, 2022.

[17] Ryan LaRose, Eleanor Rieffel, and Davide Venturelli. Mixer-phaser ansätze for quantum optimization with hard constraints. *arXiv preprint arXiv:2107.06651*, 2021.

[18] Andreas Bärtschi and Stephan Eidenbenz. Grover mixers for qaoa: Shifting complexity from mixer design to state preparation. In *2020 IEEE International Conference on Quantum Computing and Engineering (QCE)*, pages 72–82. IEEE, 2020.

[19] Austin Gilliam, Stefan Woerner, and Constantin Gonciulea. Grover adaptive search for constrained polynomial binary optimization. *Quantum*, 5:428, apr 2021.

[20] John Golden, Andreas Bärtschi, Daniel O'Malley, and Stephan Eidenbenz. Threshold-based quantum optimization. In *2021 IEEE International Conference on Quantum Computing and Engineering (QCE)*, pages 137–147, 2021.

[21] Samuel Marsh and J. B. Wang. A quantum walk-assisted approximate algorithm for bounded np optimisation problems. *Quantum Information Processing*, 18:1–18, 2019.

[22] S. Marsh and J. B. Wang. Combinatorial optimization via highly efficient quantum walks. *Physical Review Research*, 2(2), jun 2020.

[23] N. Slate, E. Matwiejew, S. Marsh, and J. B. Wang. Quantum walk-based portfolio optimisation. *Quantum*, 5:513, July 2021.

[24] Kilian Ender, Roeland ter Hoeven, Benjamin E. Niehoff, Maike Drieb-Schön, and Wolfgang Lechner. Parity quantum optimization: Compiler. 2021.

[25] Maike Drieb-Schön, Younes Javanmard, Kilian Ender, and Wolfgang Lechner. Parity quantum optimization: Encoding constraints. 2021.

[26] Michael Fellner, Kilian Ender, Roeland ter Hoeven, and Wolfgang Lechner. Parity quantum optimization: Benchmarks. 2021.

[27] Kilian Ender, Anette Messinger, Michael Fellner, Clemens Dlaska, and Wolfgang Lechner. Modular parity quantum approximate optimization. *PRX Quantum*, 3:030304, Jul 2022.

[28] Federico Dominguez, Josua Unger, Matthias Traube, Barry Mant, Christian Ertler, and Wolfgang Lechner. Encoding-independent optimization problem formulation for quantum computing. 2023.

[29] Xiaoyuan Liu, Anthony Angone, Ruslan Shaydulin, Ilya Safro, Yuri Alexeev, and Lukasz Cincio. Layer VQE: A variational approach for combinatorial optimization on noisy quantum computers. *IEEE Transactions on Quantum Engineering*, 3:1–20, 2022.

[30] Yuval R. Sanders, Dominic W. Berry, Pedro C.S. Costa, Louis W. Tessler, Nathan Wiebe, Craig Gidney, Hartmut Neven, and Ryan Babbush. Compilation of fault-tolerant quantum heuristics for combinatorial optimization. *PRX Quantum*, 1:020312, Nov 2020.

[31] B. Misra and E. C. G. Sudarshan. The Zeno's paradox in quantum theory. *Journal of Mathematical Physics*, 18(4):756–763, April 1977.

[32] Carlo Presilla, Roberto Onofrio, and Ubaldo Tambini. Measurement quantum mechanics and experiments on quantum zeno effect. *annals of physics*, 248(1):95–121, 1996.

[33] Nick Huggett. Zeno's Paradoxes. In Edward N. Zalta, editor, *The Stanford Encyclopedia of Philosophy*. Metaphysics Research Lab, Stanford University, Winter 2019 edition, 2019.

[34] P. Facchi, V. Gorini, G. Marmo, S. Pascazio, and ECG Sudarshan. Quantum zeno dynamics. *Physics Letters A*, 275(1-2):12–19, 2000.

[35] P. Facchi and S. Pascazio. Quantum zeno subspaces. *Physical Review Letters*, 89(8), aug 2002.

[36] P. Facchi and S. Pascazio. Quantum zeno dynamics: mathematical and physical aspects. *Journal of Physics A: Mathematical and Theoretical*, 41(49):493001, oct 2008.

[37] Daniel Burgarth, Paolo Facchi, Hiromichi Nakazato, Saverio Pascazio, and Kazuya Yuasa. Quantum zeno dynamics from general quantum operations. *Quantum*, 4:289, Jul 2020.

[38] Andrew M. Childs, Enrico Deotto, Edward Farhi, Jeffrey Goldstone, Sam Gutmann, and Andrew J. Landahl. Quantum search by measurement. *Phys. Rev. A*, 66:032314, Sep 2002.

[39] Dorit Aharonov and Amnon Ta-Shma. Adiabatic quantum state generation and statistical zero knowledge. *arXiv preprint arXiv:quant-ph/0301023*, 2003.

[40] R. Somma, S. Boixo, and H. Barnum. Quantum simulated annealing. *arXiv preprint arXiv:0712.1008*, 2007.

[41] R. D. Somma, S. Boixo, H. Barnum, and E. Knill. Quantum simulations of classical annealing processes. *Physical Review Letters*, 101(13), sep 2008.

[42] Sergio Boixo, Emanuel Knill, and Rolando Somma. Eigenpath traversal by phase randomization. *Quantum Info. Comput.*, 9(9):833–855, sep 2009.

[43] Yiğit Subaşı, Rolando D. Somma, and Davide Orsucci. Quantum algorithms for systems of linear equations inspired by adiabatic quantum computing. *Physical review letters*, 122(6), 2019.

[44] Lin Lin and Yu Tong. Optimal polynomial based quantum eigenstate filtering with application to solving quantum linear systems. *Quantum*, 4:361, November 2020.

[45] Lorenza Viola and Seth Lloyd. Dynamical suppression of decoherence in two-state quantum systems. *Phys. Rev. A*, 58:2733–2744, Oct 1998.

[46] P. Facchi, D. A. Lidar, and S. Pascazio. Unification of dynamical decoupling and the quantum zeno effect. *Physical Review A*, 69(3), mar 2004.

[47] Jad C. Halimeh, Haifeng Lang, Julius Mildenberger, Zhang Jiang, and Philipp Hauke. Gauge-symmetry protection using single-body terms. *PRX Quantum*, 2:040311, Oct 2021.

[48] Jad C. Halimeh, Hongzheng Zhao, Philipp Hauke, and Johannes Knolle. Stabilizing disorder-free localization. *arXiv preprint arXiv:2111.02427*, 2021.

[49] Jad C. Halimeh, Lukas Homeier, Christian Schweizer, Monika Aidelsburger, Philipp Hauke, and Fabian Grusdt. Stabilizing lattice gauge theories through simplified local pseudogenerators. *Phys. Rev. Research*, 4:033120, Aug 2022.

[50] Jad C. Halimeh, Lukas Homeier, Hongzheng Zhao, Annabelle Bohrdt, Fabian Grusdt, Philipp Hauke, and Johannes Knolle. Enhancing disorder-free localization through dynamically emergent local symmetries. *PRX Quantum*, 3:020345, May 2022.

[51] Andrew M Childs, Yuan Su, Minh C Tran, Nathan Wiebe, and Shuchen Zhu. Theory of trotter error with commutator scaling. *Physical Review X*, 11(1):011020, 2021.

[52] Andrew M Childs. Lecture notes on quantum algorithms. *Lecture notes at University of Maryland*, 2017.

[53] John Day Dollard and Charles N. Friedman. *Product Integration with Application to Differential Equations*. Encyclopedia of Mathematics and its Applications. Cambridge University Press, 1984.

[54] Jarrod R. McClean, Matthew P. Harrigan, Masoud Mohseni, Nicholas C. Rubin, Zhang Jiang, Sergio Boixo, Vadim N. Smelyanskiy, Ryan Babbush, and Hartmut Neven. Low-depth mechanisms for quantum optimization. *PRX Quantum*, 2(3), jul 2021.

[55] Yurii Nesterov. *Introductory lectures on convex optimization: A basic course*, volume 87. Springer Science & Business Media, 2003.

[56] Ryan O'Donnell. *Analysis of Boolean Functions*. Cambridge University Press, 2014.

[57] Thomas Häner, Martin Roetteler, and Krysta M. Svore. Factoring using $2n+2$ qubits with toffoli based modular multiplication. *arXiv preprint arXiv:1611.07995*, 2016.

[58] Thomas Häner, Martin Rötteler, and Krysta Marie Svore. Optimizing quantum circuits for arithmetic. *arXiv preprint arXiv:1805.12445*, 2018.

[59] Thomas Häner, Mathias Soeken, Martin Roetteler, and Krysta M. Svore. Quantum circuits for floating-point arithmetic. *arXiv preprint arXiv:1807.02023*, 2018.

[60] Craig Gidney. Halving the cost of quantum addition. *Quantum*, 2:74, jun 2018.

[61] Cody Jones. Low-overhead constructions for the fault-tolerant toffoli gate. *Physical Review A*, 87(2), feb 2013.

[62] Dmitri Maslov. Advantages of using relative-phase toffoli gates with an application to multiple control toffoli optimization. *Phys. Rev. A*, 93:022311, Feb 2016.

[63] Thomas G. Draper. Addition on a quantum computer. *arXiv preprint arXiv:quant-ph/0008033*, 2000.

[64] Lidia Ruiz-Perez and Juan Carlos Garcia-Escartin. Quantum arithmetic with the quantum fourier transform. *Quantum Information Processing*, 16(6), apr 2017.

[65] Engin S ahin. Quantum arithmetic operations based on quantum fourier transform on signed integers. *International Journal of Quantum Information*, 18(06):2050035, sep 2020.

[66] Michael A Nielsen and Isaac Chuang. *Quantum computation and quantum information*. American Association of Physics Teachers, 2002.

[67] Alex Bocharov, Martin Roetteler, and Krysta M. Svore. Efficient synthesis of universal repeat-until-success quantum circuits. *Physical Review Letters*, 114(8), feb 2015.

[68] Yunseong Nam, Yuan Su, and Dmitri Maslov. Approximate quantum fourier transform with $O(n \log(n))$ t gates. *npj Quantum Information*, 6(1), mar 2020.

[69] Robert B Griffiths and Chi-Sheng Niu. Semiclassical fourier transform for quantum computation. *Physical Review Letters*, 76(17):3228, 1996.

[70] S. Parker and M. B. Plenio. Efficient factorization with a single pure qubit and logn mixed qubits. *Physical Review Letters*, 85(14):3049–3052, oct 2000.

[71] Hayato Goto, Satoshi X. Nakamura, Mamiko Kujiraoka, and Kouichi Ichimura. Resource requirements for a fault-tolerant quantum fourier transform. *Bulletin of the American Physical Society*, 2014.

[72] Andreas Bärtschi and Stephan Eidenbenz. Short-depth circuits for dicke state preparation. *arXiv preprint arXiv:2207.09998*, 2022.

[73] Maria Schuld, Ville Bergholm, Christian Gogolin, Josh Izaac, and Nathan Killoran. Evaluating analytic gradients on quantum hardware. *Phys. Rev. A*, 99:032331, Mar 2019.

[74] David Wierichs, Josh Izaac, Cody Wang, and Cedric Yen-Yu Lin. General parameter-shift rules for quantum gradients. *Quantum*, 6:677, March 2022.

[75] M. J. D. Powell. *A Direct Search Optimization Method That Models the Objective and Constraint Functions by Linear Interpolation*. Springer Netherlands, Dordrecht, 1994.

[76] Sami Boulebna, Xavier Lucas, Agnes Meyder, Stanisław Adaszewski, and Ashley Montanaro. Peptide conformational sampling using the quantum approximate optimization algorithm. *arXiv preprint arXiv:2204.01821*, 2022.

[77] Ruslan Shaydulin, Phillip C. Lotshaw, Jeffrey Larson, James Ostrowski, and Travis S. Humble. Parameter transfer for quantum approximate optimization of weighted maxcut. *arXiv preprint arXiv:2201.11785*, 2022.

[78] Sami Khairy, Ruslan Shaydulin, Lukasz Cincio, Yuri Alexeev, and Prasanna Balaprakash. Learning to optimize variational quantum circuits to solve combinatorial problems. *Proceedings of the AAAI Conference on Artificial Intelligence*, 34(03):2367–2375, 2020.

[79] Ruslan Shaydulin and Alexey Galda. Error mitigation for deep quantum optimization circuits by leveraging prob-

lem symmetries. In *2021 IEEE International Conference on Quantum Computing and Engineering (QCE)*. IEEE, October 2021.

[80] Ashish Kakkar, Jeffrey Larson, Alexey Galda, and Ruslan Shaydulin. Characterizing error mitigation by symmetry verification in QAOA. *arXiv preprint arXiv:2204.05852*, 2022.

ACKNOWLEDGMENTS

The authors wish to thank Antonio Mezzacapo from IBM for his invaluable contributions to this project. Special thanks also to Tony Uttley, Jenni Strabley and Brian Neyenhuis from Quantinuum for their assistance on the execution of the experiments on the Quantinuum H1-2 trapped-ion quantum processor.

DISCLAIMER

This paper was prepared for information purposes with contributions from the Global Technology Applied Research center of JPMorgan Chase. This paper is not a product of the Research Department of JPMorgan Chase or its affiliates. Neither JPMorgan Chase nor any of its affiliates make any explicit or implied representation or warranty and none of them accept any liability in connection with this paper, including, but not limited to, the completeness, accuracy, reliability of information contained herein and the potential legal, compliance, tax or accounting effects thereof. This document is not intended as investment research or investment advice, or a recommendation, offer or solicitation for the purchase or sale of any security, financial instrument, financial product or service, or to be used in any way for evaluating the merits of participating in any transaction.